An H/V Geostatistical Approach for Building Pseudo-3D Vs Models to Account for Spatial Variability in Ground Response Analyses I: Model Development

Mohamad M. Hallal[1] and Brady R. Cox[2]

[1]Graduate Research Assistant, Department of Civil, Architectural and Environmental Engineering, The University of Texas at Austin, 301 E. Dean Keeton Stop C1792, Austin, TX 78712; e-mail: mhallal@utexas.edu
[2]Professor, Department of Civil, Architectural and Environmental Engineering, The University of Texas at Austin, 301 E. Dean Keeton Stop C1792, Austin, TX 78712; e-mail: brcox@utexas.edu

A non-peer-reviewed preprint uploaded to engrXiv

Abstract

Many recent studies have shown that we are generally unable to accurately replicate recorded ground motions at most borehole array sites using available subsurface geotechnical information and one-dimensional (1D) ground response analyses (GRAs). When 1D GRAs fail to accurately predict recorded site response, the site is often considered too complex to be effectively modeled as 1D. While 3D numerical GRAs are possible and believed to be more accurate, there is rarely a 3D subsurface model available for these analyses. The lack of affordable and reliable site characterization methods to quantify spatial variability in subsurface conditions, particularly regarding shear wave velocity (Vs) measurements needed for GRAs, has pushed researchers to adopt stochastic approaches, such as Vs randomization and spatially correlated random fields. However, these stochastically generated models require the assumption of generic, or assumed, input parameters, introducing significant uncertainties into the site response predictions. This paper describes a new geostatistical approach that can be used for building pseudo-3D Vs models as a means to rationally account for spatial variability in GRAs, increase model accuracy, and reduce uncertainty. Importantly, it requires only a single measured Vs profile and a number of simple, cost-effective, horizontal-to-vertical spectral ratio (H/V) noise measurements. Using Gaussian geostatistical regression, irregularly sampled estimates of fundamental site frequency from H/V measurements ($f_{0,H/V}$) are used to generate a uniform grid of $f_{0,H/V}$ across the site with accompanying Vs profiles that have been scaled to match each $f_{0,H/V}$ value, thereby producing a pseudo-3D Vs model. This approach is demonstrated at the Treasure Island and Delaney Park Downhole Array sites (TIDA and DPDA, respectively). While the pseudo-3D Vs models can be used to incorporate spatial variability into 1D, 2D, or 3D GRAs, their implementation in 1D GRAs at TIDA and DPDA is discussed in a companion paper.

Introduction

Many recent studies (e.g., Afshari and Stewart, 2019; Kaklamanos et al., 2013, 2015; Kaklamanos and Bradley, 2018; Tao and Rathje, 2019; Teague et al., 2018; Thompson et al., 2009, 2012; Zalachoris and Rathje, 2015) have shown that we are generally unable to accurately replicate recorded ground motions at most borehole array sites using available subsurface geotechnical information and one-dimensional (1D) ground response analyses (GRAs). When 1D GRAs fail to accurately predict recorded site response, the site is often considered too complex to be effectively modeled as 1D. While 3D numerical GRAs are possible and believed to be more accurate, there is rarely a 3D subsurface model available for these analyses. The lack of affordable and reliable site characterization methods to quantify spatial variability in subsurface conditions, particularly regarding shear wave velocity (Vs) measurements needed for GRAs, is an impediment to future progress in accurate site response modeling. Indeed, even at our most valued downhole array sites in the U.S., Japan, and elsewhere globally, we are generally limited to 1D representations of Vs.

Common Vs characterization techniques can be subsumed under two categories: invasive/borehole methods and noninvasive/surface wave methods. Invasive methods (e.g., downhole, crosshole, PS logging) require placing the seismic source and/or receiver(s) in the subsurface material being characterized. These methods produce 1D Vs profiles at the measurement location that are generally believed to be more accurate than those from noninvasive methods, even though they are often more time consuming and expensive. Noninvasive methods (e.g., active- and passive-surface wave measurements, full waveform inversion) use arrays of receivers placed across the ground surface, and thus sample a broader spatial area. However, most surface wave approaches rely on the basic assumption that the medium beneath the array can be approximated by 1D geometry (Foti et al., 2011). In the presence of variable subsurface conditions, surface wave methods result in a complex averaging of material properties beneath the array. This fact, combined with the nonunique nature of the surface wave inverse problem, results in 1D Vs profiles that are generally believed to be less accurate than those from invasive methods, even though they are often a cost and time efficient alternative for deep profiling.

Regardless of whether invasive or noninvasive methods are used for dynamic site characterization, typically a single deterministic 1D Vs profile is obtained for each measurement location. In the absence of additional information, these 1D Vs profiles are used to perform 1D GRAs, which assume that all subsurface layers are isotropic, laterally homogeneous, and extend infinitely. Researchers have shown that these assumptions greatly limit the effectiveness of 1D GRAs due to the laterally variable conditions characterizing the shallow geology of most sites (Afshari and Stewart, 2019; Assimaki et al., 2003; Kaklamanos and Bradley, 2018; Tao and Rathje, 2019; Thompson et al., 2009, 2012). Depending on the extent of spatial variability, 1D GRAs can be inadequate and incapable of capturing complex effects, such as wave scattering, locally generated surface waves, and basin effects, among others (Kaklamanos et al., 2013).

In an attempt to replicate the inherent spatial variability in Vs within the 1D GRA framework, researchers proposed using probabilistic statistical models (e.g., Toro, 1995) to randomly vary the properties of a reference 1D Vs profile (Kaklamanos and Bradley, 2018; Rathje et al., 2010; Tao and Rathje, 2019). While this approach still relies on 1D GRAs with assumed laterally homogeneous subsurface layers, the combined result of all randomly generated Vs profiles can reproduce wave scattering effects (Nour et al., 2003). However, this method relies on stochastic probabilistic modeling approaches and requires site-specific input parameters that are not typically available, bringing additional uncertainty to the predictions (Passeri et al., 2019; Teague et al., 2018). This uncertainty can be significant, and blind Vs randomization has been shown to yield unrealistic Vs profiles that lead to poor site response predictions (Griffiths et al., 2016a, 2016b) that are different than ground motions recorded at downhole array sites (Teague et al., 2018). Additionally, even if randomization methods can reproduce wave scattering effects, other complex phenomena caused by highly variable subsurface conditions cannot be captured.

Recognizing the imperfect ability of modified 1D GRAs to account for 3D spatial variability, advanced 2D/3D GRAs are slowly gaining popularity. Such analyses require accurate information on the 2D/3D geometry and material properties of the subsurface, specifically the Vs. Within this context, several methods for constructing 2D/3D Vs models using in-situ measurements have been developed. The simplest approach is to utilize multiple spatially distributed 1D Vs profiles to construct pseudo-2D (e.g., Luo et al., 2008; Mi et al., 2017; Parolai et al., 2001) and 3D (e.g., Pan et al., 2018; Piatti et al., 2013; Strobbia et al., 2011) Vs models by spatial interpolation techniques. For example, this approach has been applied to construct pseudo-2D Vs profiles from multi-channel analysis of surface waves (MASW) by interpolating a series of 1D Vs models derived from inversion of waveforms collected using different receiver arrays (e.g., Ismail et al., 2014; Mahvelati and Coe, 2017; Park, 2005). While this method can be used to produce pseudo-2D/3D Vs models, the input 1D velocity profiles represent spatial averages over the length of the receiver array, leading to limited resolution. Additionally, this method requires significant numbers of array/Vs measurement locations with good azimuthal coverage around the site, which renders it extremely time consuming and cost prohibitive.

Other methods have been proposed to obtain true 2D/3D Vs models with higher resolution, with the most common being tomography and full waveform inversion (FWI). Tomographic methods are based on cross-correlating and summing ambient noise measurements from pairs of sensors to assemble 2D frequency-dependent group or phase velocity maps, which are then inverted to obtain 3D Vs models. The method has been applied on continental and regional scales using very low frequency waves to image the Earth's crust and upper mantle (Chen et al., 2018; Ritzwoller and Levshin, 1998; Yang et al., 2007) and has been extended to higher frequencies to image the near surface Vs at local scales (Picozzi et al., 2009; Pilz et al., 2012). Rather than inverting dispersion information, FWI attempts to reconstruct the subsurface model that could produce theoretical waveforms matching the entire wavefield measured by a large array of sensors. This requires a full solution of the governing wave equation in 3D. The approach has been applied to characterize the near surface Vs and detect anomalies, such as voids, among other applications (Kallivokas et al., 2013; Tran et al., 2013; Tran and Sperry, 2018).

Both methods, however, require solving large inverse problems, which are nonlinear, ill-posed, and nonunique (Pan et al., 2019; Pilz et al., 2012; Virieux and Operto, 2009). Additionally, in processing and inverting data from tomography, many critical assumptions are made, including, great-circle (i.e., approximately straight) propagation path between sensor pairs, lateral smooth variation of Vs, and uniform distribution of ambient noise. These assumptions are generally violated, which has been shown to introduce bias into tomography (Chen et al., 2018; Picozzi et al., 2009; Ritzwoller and Levshin, 1998; Yang et al., 2007). FWI also faces challenges pertaining to inconsistent source excitation, variable coupling of sensors, lack of low-frequency waves, and high computational complexity in terms of both time and memory (Tran et al., 2013; Tran and Sperry, 2018; Virieux and Operto, 2009). Finally, the need for wide-aperture surveys with numerous, simultaneously recording sensors, which is not practical in urban areas, is another limitation for both tomography and FWI. For these reasons, these methods are seldom applied to obtain 2D/3D Vs models for ground motion studies in practice.

The lack of affordable and reliable 3D characterization methods, particularly regarding Vs measurements, has pushed researchers to adopt stochastic approaches to construct 2D/3D Vs models for GRAs. Using a single 1D Vs profile, 2D/3D Vs models are developed by continuously perturbing the 1D information to mimic continuous spatial variability. Stochastic probabilistic modeling approaches have been widely used for this purpose in geotechnical earthquake engineering. The most widely used probabilistic modeling approach utilizes spatially correlated random fields to introduce randomness to a baseline 1D Vs model (e.g., de la Torre et al., 2019; Thompson et al., 2009). While conceptually simple, generating 3D spatially correlated random fields is numerically and computationally intensive (Thompson et al., 2009), especially considering that several randomly generated realizations of the subsurface conditions may be needed to assess the uncertainty. Also, similar to 1D Vs randomization methods, these stochastically generated 2D/3D models require the assumption of generic input parameters derived for other sites, which may not be able to account for the site-specific spatial variability in a meaningful way. This inevitably introduces significant uncertainties into the predictions.

The collective result of the issues presented above demonstrates the need for an affordable method to construct Vs models which account for site-specific spatial variability using approaches that: (1) are not fully stochastic, but site-specific, (2) do not require inputs that cannot be known a priori, and (3) can conveniently develop Vs models over large areas (hundreds of square meters) without significant acquisition and processing efforts. This paper presents a new framework called the 'H/V geostatistical approach' that can be used to develop site-specific pseudo-3D Vs models in a rigorous and simple manner. The proposed approach distinguishes itself from previous studies in three key ways: (1) it requires only a single, accurately measured Vs profile down to engineering bedrock, (2) it relies majorly on estimates of fundamental site frequency (f_0; a key parameter governing site effects) obtained from simple horizontal-to-vertical spectral ratio (H/V) noise measurements ($f_{0,H/V}$), and (3) it creates models that can be used to ensure proper incorporation of site-specific spatial variability in 1D, 2D, and 3D GRAs. In a companion paper (Hallal and Cox, 2020), the benefits of implementing the pseudo-3D Vs models generated using the proposed approach in 1D GRAs are discussed.

In this paper, we first discuss the theory behind H/V measurements and their use for inferring subsurface properties. Second, we describe the general framework of the proposed H/V geostatistical approach in terms of generating a uniform grid of $f_{0,H/V}$ across a certain area with accompanying Vs profiles that have been scaled from the measured Vs to match each $f_{0,H/V}$ value, thereby producing a pseudo-3D Vs model. Third, we summarize information on two case study sites, the Treasure Island Downhole Array (TIDA) and Delaney Park Downhole Array (DPDA), along with the field studies used to measure the spatial variability of f_0 across each site using widely distributed, noninvasive H/V measurements. Fourth, we present the application of the H/V geostatistical approach for building pseudo-3D Vs models at the two case study sites. Fifth, we discuss the descriptive measures/statistics of the site-specific spatial variability that should be properly accounted for and conclude with final remarks.

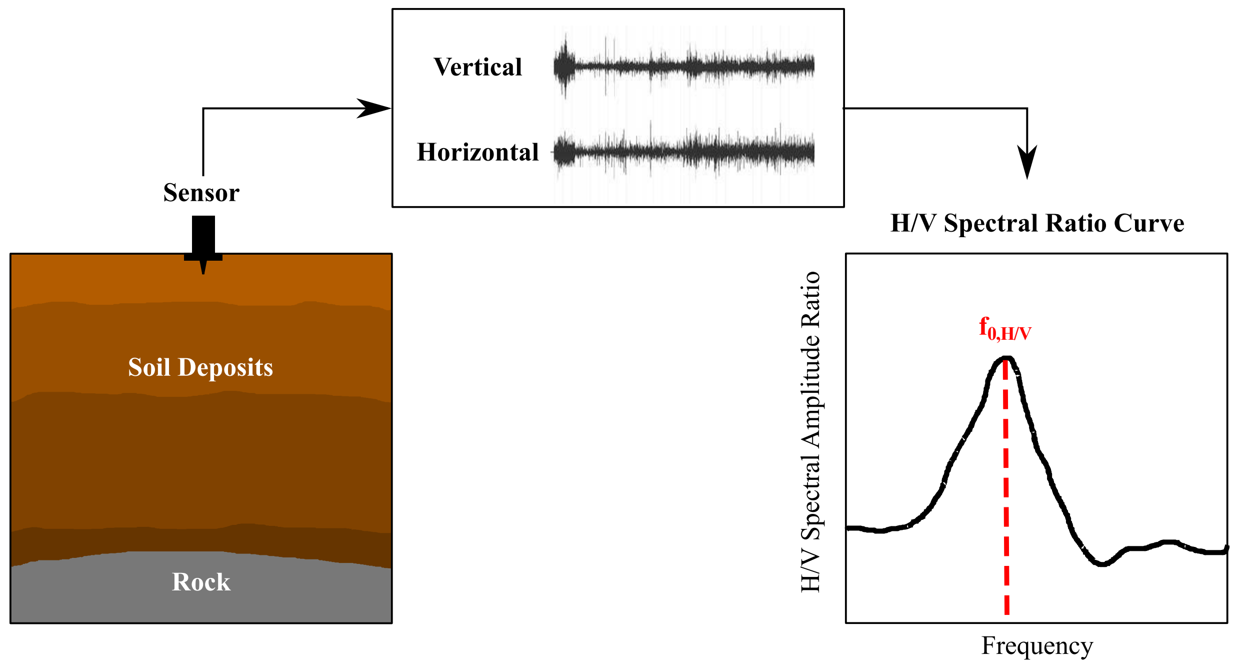

Figure 1. Simplified schematic of the horizontal-to-vertical spectral ratio (H/V) method used to infer the fundamental site frequency ($f_{0,H/V}$).

Review on H/V Theory

The novelty of the proposed approach comes from the integration of H/V measurements and their strong dependence on subsurface conditions controlling site response with geostatistical modeling tools. A major component of the proposed approach is performing a number of spatially distributed H/V measurements across and around the site in order to capture trends in the variation of f_0. The H/V method, which was first proposed by Nogoshi and Igarashi (1971) and later popularized by Nakamura (1989), is continuously attracting more and more interest in seismic studies due to its recognized ability to estimate f_0 for sites with a strong impedance contrast in a cost-effective, time-efficient, and feasible way. As shown in Figure 1, the H/V method utilizes ambient noise recordings (generally, 15- to 30-minute time records are sufficient) from the horizontal and vertical components of a single, three-component seismometer to estimate f_0. The H/V curves are computed as the ratio of the Fourier amplitude spectra (FAS) of the horizontal and vertical components of the noise record. While each horizontal component can be considered separately, or rotated to a particular orientation based on horizontal polarization analyses, it is most common to combine the two horizontal components using one of several methods (Albarello and Lunedei, 2013; Cox et al., 2020; Fäh et al., 2001; Haghshenas et al., 2008).

Experimental and theoretical studies have shown that if the H/V spectral ratio curve of ambient noise exhibits a dominant, well-defined peak (or multiple clear peaks, if multiple strong impedance contrasts are present at different depths), then the lowest frequency peak can be used to infer the fundamental shear wave resonance frequency at the location of the recording seismometer (Bard and SESAME-Team, 2004; Lachet and Bard, 1994; Lermo and Chavez-Garcia, 1993). Owing to this simple acquisition and processing, many spatially distributed H/V measurements can easily be conducted across a site of interest as a means to infer the variation of fundamental site frequency. As fundamental site frequency is being estimated from H/V measurements, we refer to it as $f_{0,H/V}$.

Several competing theories exist regarding the basis for the relation between $f_{0,H/V}$ and f_0. One theory hypothesizes that the H/V spectral ratio curve is a proxy to the Rayleigh wave ellipticity curve, which is simply the ratio of the amplitude of the horizontal particle motion to that of the vertical particle motion (Fäh et al., 2003; Lachet and Bard, 1994). However, the validity of this hypothesis depends on the composition of the ambient noise wavefield. If the wavefield is composed exclusively of fundamental mode Rayleigh waves, then the H/V spectral ratio curve is equivalent to the ellipticity curve. In reality, the wavefield includes different modes of Rayleigh, Love, and body waves, which are generally not separated in time. Owing to this complex wavefield composition, the H/V spectral ratio curve will not exactly represent the ellipticity curve. If the energy partition between the different waves is known, the H/V spectral ratio curve can be corrected to obtain ellipticity (Hobiger et al., 2013; Scherbaum et al., 2003). However, studies have shown that the energy partition varies from site to site and, even for a given site, is frequency-dependent and changes with time, making the H/V correction a nontrivial task (Endrun, 2011). Directly extracting the Rayleigh wave ellipticity would avoid making any assumptions on the composition of the wavefield (Hobiger et al., 2013). However, a further evaluation of this issue is beyond the scope of this paper.

Evaluating the contribution of different wave types is critical to applications that attempt to invert H/V spectral ratios to retrieve the Vs profile. It is well established that the frequency-dependency of ellipticity is linked to the Vs profile, and by using its relation to the H/V curve, many researchers have used the H/V curve to obtain Vs profiles directly via inversion (e.g., Parolai et al., 2001; Yamanaka et al., 1994). However, inaccurate identification of the proportion of fundamental mode Rayleigh waves might severely bias the inversion (Bonnefoy-Claudet et al., 2006). Additionally, the H/V curve is dimensionless, causing the inversion to be subject to a strong tradeoff between the layers' thicknesses and Vs (Scherbaum et al., 2003; Yamanaka et al., 1994). That is, by scaling the wave velocities and layer thicknesses by the same constant, the ellipticity curve remains exactly the same (Hobiger et al., 2013). It is thus obvious that an H/V curve alone is not sufficient to obtain the Vs profile, and additional information, such as wave velocities, layer thicknesses, or dispersion estimates, is needed.

Regardless of the composition of the wavefield, researchers have shown that the position of the H/V spectral ratio peak is unaffected (Bonnefoy-Claudet et al., 2006). Thus, whatever the predominant wave type is, H/V spectral ratio curves can be used to infer the fundamental shear wave resonance frequency, at least for sites with a strong impedance contrast. Therefore, we hereafter focus on common methods used to obtain $f_{0,H/V}$ and its relation to subsurface conditions. Although relatively simple calculations are required for the H/V technique, there exist several deterministic and statistical methods to obtain the $f_{0,H/V}$ (Cox et al., 2020). Cheng et al. (2020) summarized the existing techniques and proposed a new method that directly accounts for azimuthal variability, as several studies have shown the existence of azimuthal variability in $f_{0,H/V}$ and attribute it to anisotropic ambient vibration sources and/or complex subsurface conditions which do not fall under the idealized 1D assumptions.

If H/V measurements are performed at multiple locations, the extent to which the $f_{0,H/V}$ varies across the area of interest can be examined and mapped in 2D. The spatial variability of $f_{0,H/V}$ reflects the degree of variability in the subsurface Vs structure that governs site response. This includes variations in the Vs of soil layers, their thicknesses, and/or in the depth to a major impedance contrast. Potential causes for changes in $f_{0,H/V}$ can be inferred by examining the equation of the fundamental site frequency of a single representative soil layer with an average shear wave velocity ($Vs_{,avg}$) and thickness (H) overlying a rigid half-space. For such conditions, f_0 can be approximated from the quarter-wavelength relationship, as shown in Equation 1. It is intuitive from this equation that f_0 is directly proportional to Vs but inversely proportional to the depth to a major impedance contrast, which is typically that of the soil-rock interface. Thus, an increase in f_0 is associated with shallower rock and/or an overall stiffer soil column, and vice versa. This relationship forms the basis for the H/V geostatistical approach proposed herein to build pseudo-3D Vs models.

$$f_0 \cong \frac{V_{S,avg}}{4H} \tag{1}$$

H/V Geostatistical Approach for Building Pseudo-3D Vs Models

The H/V geostatistical approach proposed herein uses site-specific, simple measurements to develop a reasonable and representative pseudo-3D subsurface model that can be used to incorporate spatial variability into 1D, 2D, and 3D GRAs. The site characterization information required to implement this approach is: (1) at least one Vs profile down to engineering bedrock (i.e., the impedance contrast governing f_0 and site response), and (2) a number of H/V measurements spatially distributed across the site. The appropriate number of H/V measurements will depend on the size and complexity of the site, but should be sufficient to capture trends in the variation of f_0 across the site. Additionally, it may be necessary to conduct H/V measurements outside the proper boundaries of your site in order to capture spatial variability over the area that is impacting site response. Insights into the area required to account for spatial variability in GRAs are discussed in Hallal and Cox (2020).

A schematic summary of the H/V geostatistical approach is shown in Figure 2. First, the irregularly spaced $f_{0,H/V}$ measurements are interpolated (for example, using kriging) to obtain a uniformly estimated map of $f_{0,H/V}$ values. Second, using the $f_{0,H/V}$ value closest to the measured Vs profile ($f_{0,H/V,Vs}$) and the estimated $f_{0,H/V}$ map, a uniformly estimated scaling factor (S_{f_0}) map is obtained. Finally, a spatially variable pseudo-3D Vs model is built on the same uniform grid by multiplying the layer thicknesses of the measured Vs profile by S_{f_0} of each cell. The application could be easily extended to include multiple measured Vs profiles if desired. The pseudo-3D Vs model can be visualized by stacking the scaled Vs profiles from all cells in 1D, by plotting 2D Vs cross sections along certain azimuths, or by viewing different cross sections in 3D (refer to Figure 2). The methodology is explained in greater detail in the subsequent subsections and then demonstrated for two downhole array case study sites.

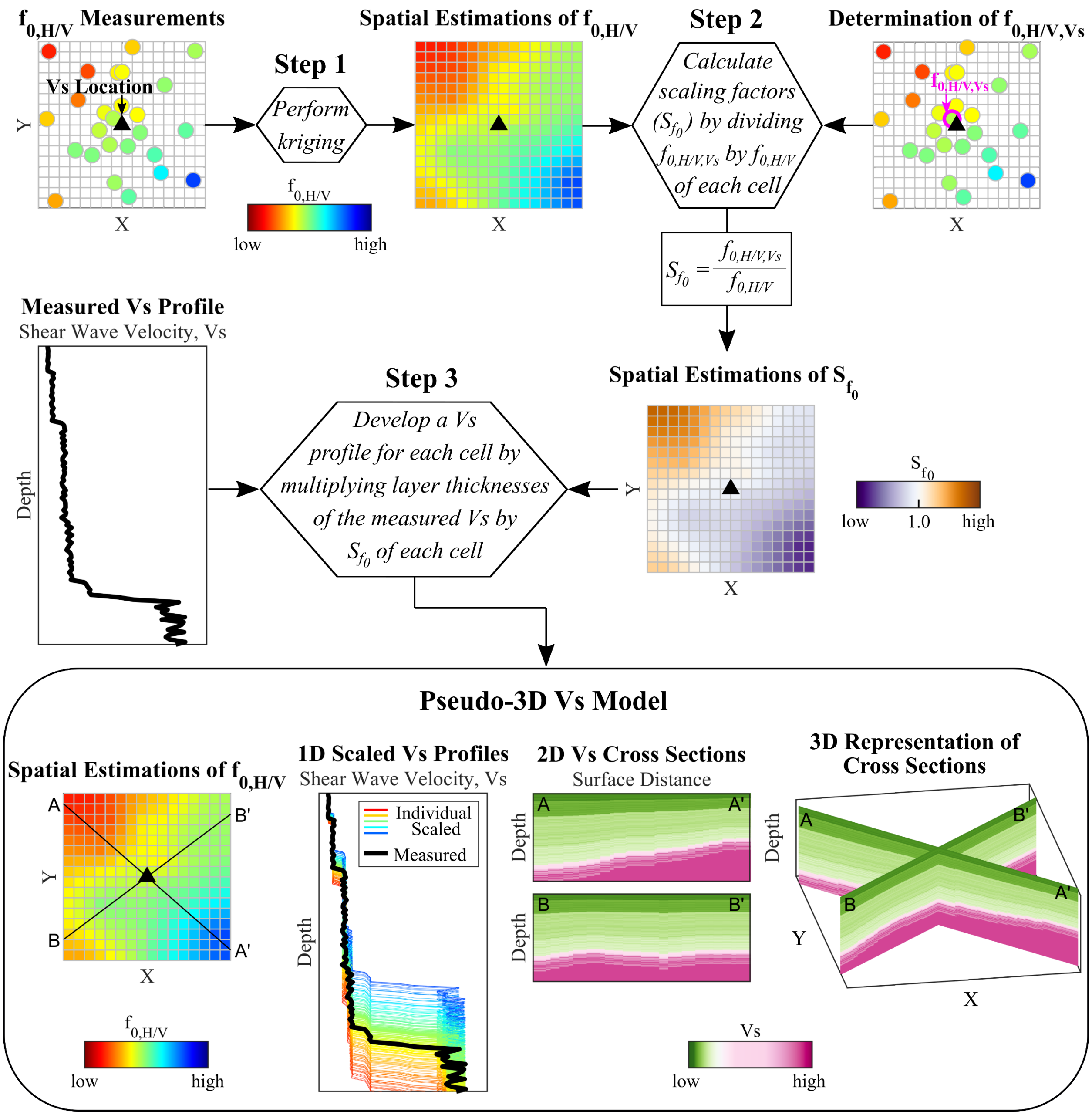

Figure 2. Schematic representation of the H/V geostatistical approach proposed herein to build pseudo-3D Vs models that can be used to incorporate spatial variability into ground response analyses.

Uniform Spatial Estimation of $f_{0,H/V}$

The first step in the proposed approach aims at uniformly mapping the variation of $f_{0,H/V}$ over an area of interest using irregularly sampled H/V measurements. Exhaustive measurements on a uniform grid are not practical, or even possible due to access and/or budget limitations, and thus irregular spatial sampling is always performed. The $f_{0,H/V}$ values at unsampled locations are then obtained via spatial estimation methods. An in-depth assessment of different estimation techniques is beyond the scope of this paper and we only provide a systematic method rather than the "best" one for the desired application. Ultimately, individual users can judge which spatial estimation technique is best for their application. In this study, we use the kriging with a trend approach, also known as kriging after detrending (Hengl et al., 2004; Isaaks and Srivastava, 1989). Compared to other methods, kriging has the advantage of incorporating valuable information regarding the site-specific spatial correlation and anisotropy, in addition to minimizing the error of the estimated values. Moreover, combining kriging with a trend has been proven to yield more accurate results, especially for geotechnical-related applications, where the data sets nearly always show some pattern of spatial continuity related to geology (Hengl et al., 2004; Isaaks and Srivastava, 1989).

The estimated $f_{0,H/V}$ map is obtained in a two-step approach, in which the trend and residuals are fitted separately and then summed. We model the trend in the $f_{0,H/V}$ values using a convolution-based method, which is a moving window average of the measurements. The trend is then subtracted from the data and ordinary kriging is performed on the residuals. This step requires modeling the spatial correlation of the measurements, or its reverse, which is commonly done using the semivariogram. The semivariogram is a measure of the degree of variability between observations as a function of their separation distance. Kriging on the residuals is then performed on a grid with a specified cell size. We use 50-m cells herein, however smaller cell sizes might be needed for sites which show significant spatial variability within small distances. After performing kriging to map the residuals over a uniform area, the trend is added (Isaaks and Srivastava, 1989) and the final output is a uniformly estimated $f_{0,H/V}$ map.

Building a Pseudo-3D Vs Model

The uniformly estimated $f_{0,H/V}$ map is only a means to develop a pseudo-3D subsurface model that captures the key aspects of the site-specific spatial variability likely to influence site response. To achieve this, a single measured Vs profile is repeatedly modified/scaled for each cell such that the modified profile is consistent with the $f_{0,H/V}$ value of that cell. The task of perturbing the Vs profile to match $f_{0,H/V}$ is not trivial, as changes in $f_{0,H/V}$ result from variations in the layers' Vs, their thicknesses, and/or the depth to the major impedance contrast (refer to Equation 1). If we make the simplifying assumption that the layer thicknesses and depth to the major impedance contrast are primarily controlling the change in $f_{0,H/V}$, then the individual layer thicknesses can be altered to achieve the desired $f_{0,H/V}$. While this assumption inherently includes some uncertainty, it provides a feasible way of economically developing representative Vs profiles over a large footprint. Additionally, previous research has shown that if Vs profiles match the experimental site signature, which is implemented here by targeting $f_{0,H/V}$, then the uncertainty in GRAs is greatly reduced (Griffiths et al., 2016a; Teague et al., 2018).

Since we are scaling the measured Vs profile to a target $f_{0,H/V}$ at each grid point, we need to represent the measured Vs profile with an $f_{0,H/V}$ value, which we refer to as $f_{0,H/V,Vs}$. The $f_{0,H/V,Vs}$ is simply obtained from the H/V measurement closest to the location of the measured Vs profile (Figure 2). By having an initial $f_{0,H/V,Vs}$ and a target $f_{0,H/V,i}$ for the i^{th} cell in the grid, we can compute a simple scaling factor as the ratio of these two values for that cell ($S_{f_{0,i}}$), as shown in Equation 2.

$$S_{f_{0,i}} = \frac{f_{0,H/V,V_s}}{f_{0,H/V,i}} \cong \frac{\left(\frac{V_{S,avg}}{4H}\right)_{V_s}}{\left(\frac{V_{S,avg}}{4H}\right)_i} = \frac{\frac{V_{S,avg}}{4H_{V_s}}}{\frac{V_{S,avg}}{4H_i}} = \frac{H_i}{H_{V_s}} \tag{2}$$

Vs profiles are finally developed for each cell by simply multiplying the layer thicknesses of the measured Vs profile by $S_{f_{0,i}}$ of each cell (Figure 2). This ensures that the thickness of the soil above the major impedance contrast of the measured Vs profile (H_{Vs}) will be scaled by $S_{f_{0,i}}$ and consequently, as shown in Equation 2, $f_{0,H/V,Vs}$ will be scaled by $1/S_{f_{0,i}}$, achieving the target $f_{0,H/V,i}$. This is true because we are assuming that the measured Vs remains constant for each layer and that the thicknesses of all layers are estimated by the same scaling factor, implying that the $Vs_{,avg}$ of the soil column above the major impedance contrast also remains constant for all cells.

We acknowledge that although variability in the layers' Vs or thickness scaling can be introduced, this causes the problem of modifying the Vs profile to be ill-posed with infinite possibilities. To avoid the need to account for this non-uniqueness and additional uncertainty, we decided not to include it as part of this study. One approach to avoid assuming either constant Vs or constant thickness scaling for each layer is to invert the measured H/V curves while keeping the layers' thicknesses or Vs fixed, respectively. Recall that inverting the H/V curve alone is not sufficient to uniquely determine the Vs profile, and generally either the layers' thicknesses or Vs must be fixed while the other parameter is inverted for. However, this still requires correcting the H/V curve to obtain ellipticity by assuming the energy partition of waves. Another limitation of inverting the H/V curves is that Vs profiles can only be inverted at H/V measurement locations rather than over a uniform grid. This is true because H/V curves at unsampled locations cannot be estimated; we only estimate $f_{0,H/V}$ values at unsampled locations rather than the full H/V curve. Thus, this approach will further require interpolating the Vs profiles inverted at each H/V measurement location, which are spatially irregular, to obtain a pseudo-3D Vs model. Future research on this topic will be required. As shown in the accompanying paper, the simple scaling approach used herein provides Vs models that work well for integrating site-specific spatial variability into GRAs.

Information on Case Study Sites

The proposed H/V geostatistical approach is validated at two downhole array sites, the TIDA and DPDA. In this paper, we only discuss the development of the pseudo-3D Vs models at both sites and assess them in light of available geologic information. In a companion paper (Hallal and Cox, 2020), the pseudo-3D Vs models are used to account for spatial variability in 1D GRAs and the results are compared to recorded ground motions for validation. The two downhole array sites were selected to represent two distinct geographic and geologic conditions. Importantly, TIDA is believed to be an archetype of 1D conditions, whereas DPDA is the antithesis of such conditions (Tao and Rathje, 2019). For each site, the geology and subsurface properties are described in what follows, along with the H/V measurements.

Treasure Island Downhole Array

The TIDA site is located in a seismically active region of northern California, approximately 5 km northeast of San Francisco, 12 km west of the Hayward fault, and 20 km east of the San Andreas fault. The downhole array is deployed in an artificial hydraulic fill island constructed on a natural sandspit northwest of Yerba Buena Island (YBI), an outcropping bedrock island in San Francisco Bay (Rollins et al., 1994). A simplified stratigraphy for TIDA is shown in Figure 3a along with the depths of the triaxial ground motion accelerometers, as indicated by the black

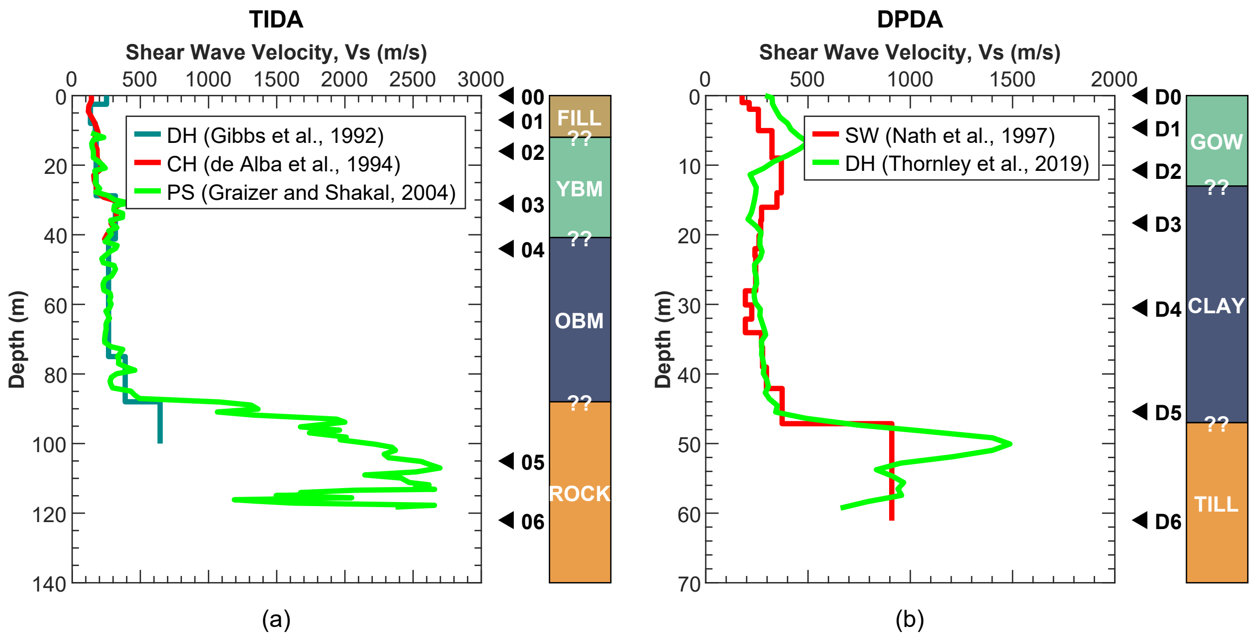

Figure 3. Measured Vs profiles, triaxial accelerometer sensor depths (black triangle symbols), and simplified stratigraphy at: (a) the Treasure Island Downhole Array (TIDA), and (b) Delaney Park Downhole Array (DPDA) sites. The measured Vs profiles at TIDA are from seismic downhole (DH) (Gibbs et al., 1992), shallow crosshole (CH) (de Alba et al., 1994), and deep PS suspension logging (Graizer and Shakal, 2004) and the stratigraphy is based on Gibbs et al. (1992). The measured Vs profiles at DPDA are from inversion of surface wave data (SW) (Nath et al., 1997) and seismic downhole (DH) (Thornley et al., 2019) and the stratigraphy is based on geologic cross sections from Combellick (1999).

triangle symbols. Existing data indicates that the subsurface near the downhole array site consists of around 15 m of loose sandy hydraulic fill, followed by approximately 15 m of Young San Francisco Bay Mud. The Young Bay Mud (YBM) is underlain by silty sand, Old Bay Mud (OBM), and a mixture of gravel, sand, and clay, all of which are sedimentary deposits of Quaternary age. The bedrock is located at approximately 90 m and is composed of interbedded sandstone, siltstone, and shale of the Franciscan Formation, which is of Jurassic-Cretaceous age (Gibbs et al., 1992; Pass, 1994).

The site has been characterized through several geotechnical testing programs, including Vs measurements performed using multiple invasive borehole methods. The Vs profiles compared in Figure 3a include measurements from seismic downhole (Gibbs et al., 1992), shallow crosshole (de Alba et al., 1994), as well as deep PS suspension logging (Graizer and Shakal, 2004). The tests were performed in close vicinity to one another, all within an area of approximately 40 m^2. The seismic downhole and PS suspension logging Vs profiles indicate a transition from soil to rock at approximately 90 m. However, the PS suspension logging profile shows a significantly higher bedrock Vs compared to the seismic downhole measurements. The seismic downhole report mentions that wave arrivals in rock were obscure due to poor energy transmission and wave interference (Gibbs et al., 1992). Because of this uncertainty and the limited depth of the crosshole testing, only the PS suspension log is used throughout this study for the TIDA site.

Delaney Park Downhole Array

The DPDA site is located in southern Alaska in one of the most seismically active regions in the U.S. Seismicity in this area is influenced by the Castle Mountain fault, Bruin Bay fault, Border Ranges fault, several faults in Cook Inlet, and the Aleutian megathrust subduction zone (Wen and Kalkan, 2017). The downhole array is deployed in Delaney Park in downtown Anchorage, which is a lowland area west of the Chugach Mountains. A simplified soil profile for DPDA is shown in Figure 3b (Combellick, 1999) along with the depths of the triaxial ground motion accelerometers. Geologic data indicates that the subsurface near the downhole array site consists of around 15 m of glacial outwash (GOW), followed by approximately 30 m of clay from the Bootlegger Cove Formation, overlying glacial till. The glacial till is located at approximately 47 m and consists of very dense sand and gravel. All these deposits are of Quaternary age and are underlain by thick Tertiary sediments of sandstone, siltstone, and claystone. The Tertiary deposits in Anchorage are located starting between 100 and 300 m below the surface and are a few kilometers thick (Badal et al., 2004; Combellick, 1999).

Prior to 2019, no Vs measurements had been conducted in the immediate vicinity of the DPDA site. Thus, the only Vs profile available for GRAs was from the inversion of surface wave data collected by Nath et al. (1997) at a site approximately 250 m away. More recently, Thornley et al. (2019) performed seismic downhole measurements in the borehole of the deepest DPDA accelerometer. The Vs profiles by Nath et al. (1997) and Thornley et al. (2019) extend approximately 60 m into the Quaternary deposits, as shown in Figure 3b. While the comparison shows differences in the Vs over the top 15 m, both profiles indicate a transition from soft soil to hard till (engineering rock-like material) at a depth of approximately 47 m. However, only the seismic downhole profile is used throughout this study for the DPDA site since Thornley et al. (2019) reported that it provides an improvement in the site response predictions over the previous profile and it is in closer vicinity to the borehole array.

H/V Measurements

To efficiently characterize the spatial variability over a wide area around the downhole array sites, surface-based seismic measurements were conducted. Specifically, ambient vibrations were recorded using broadband seismometers deployed as part of both surface wave Microtremor Array Measurements (MAM) and single-station deployments; herein we only discuss the H/V results. Because azimuthal variability in H/V might be of interest in the present study, the $f_{0,H/V}$ were obtained following the procedures proposed by Cheng et al. (2020). Using measurements from the two perpendicular horizontal components (i.e., NS and EW), horizontal motions at six different azimuths spaced at 30° were calculated using horizontal polarization analysis. The ambient noise records were divided into many 60-sec time windows and a frequency-domain window-rejection algorithm was used to remove contaminated time windows, as discussed in Cox et al. (2020). Then, for each azimuth and time window, an H/V spectral ratio curve was computed as the ratio of the FAS of the windowed azimuthal horizontal motion to that of the vertical motion and an $f_{0,H/V}$ value was obtained from the amplitude of the lowest frequency peak. The representative $f_{0,H/V}$ is finally taken as the lognormal-median of the $f_{0,H/V}$ values of all azimuths and all time windows at the location of the H/V measurement. While this lognormal-median value that accounts for azimuthal variability will be referred to herein as $f_{0,H/V}$ for simplicity, it is more rigorously notated as $LM_{f_{0,AZ}}$ by Cheng et al. (2020).

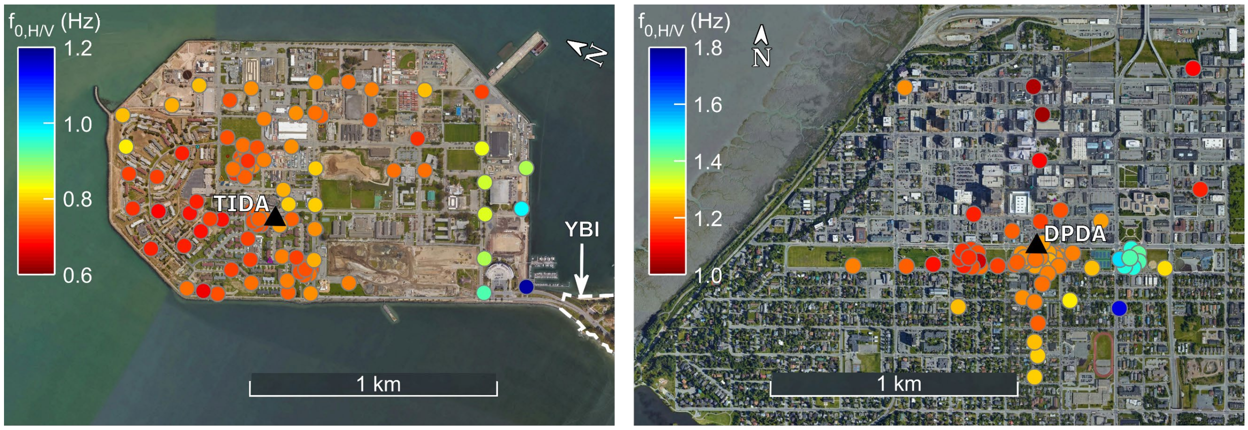

(a) (b)

Figure 4. Fundamental site frequency map inferred from H/V measurements ($f_{0,H/V}$) across the: (a) TIDA, and (b) DPDA sites. The location of the downhole array at each site is denoted with a black triangle.

A map showing the variation in $f_{0,H/V}$ obtained from H/V measurements at 97 locations around the TIDA site is shown in Figure 4a. The $f_{0,H/V}$ values are quite consistent across most of the island and equal to approximately 0.75 – 0.80 Hz. However, the values increase abruptly in the south where bedrock shallows near the causeway to YBI. Treasure Island was constructed in an estuarine depositional environment, which is generally characterized by a uniform deposition of sediments (Tao and Rathje, 2019). It follows that if minimal variability exits in the fundamental frequency and in surficial soil layers, then based on Equation 1, the depth to bedrock is also expected to be generally uniform. As discussed earlier, an increase in the fundamental frequency is attributed to an increase in the average Vs and/or a decrease in the depth to bedrock. We believe that the major contributor to the rapid increase in $f_{0,H/V}$ is shallower bedrock, which is expected as the rocks of the Franciscan Formation slope upward and ultimately outcrop on YBI.

The mapped spatial distribution of $f_{0,H/V}$ inferred from 96 H/V measurements around the DPDA site is shown in Figure 4b. Unlike TIDA, the distribution of the $f_{0,H/V}$ values shows considerable heterogeneity in almost all lateral directions. The heterogeneity is minimal in close vicinity to the downhole array, but becomes more significant in as little as 300 m away. The $f_{0,H/V}$ values decrease in the north direction but increase in the south-east quadrant. This variability is expected in a glacial depositional environment, in which glacial movements lead to variable geologic features on the order of tens to hundreds of meters (Tao and Rathje, 2019). It is expected that lower frequencies correspond to deeper glacial till in the north direction and higher frequencies correspond to shallower glacial till in the east direction. However, while the depth to the glacial till might be driving the change in $f_{0,H/V}$, we also expect variations in the thickness and Vs of the surficial layers to play a role.

Implementation at Case Study Sites

This section presents the implementation of the proposed H/V geostatistical approach at the TIDA and DPDA sites. First, the $f_{0,H/V}$ measurements are kriged to obtain a uniformly estimated $f_{0,H/V}$ map using the kriging with a trend approach. Second, the uniformly estimated $f_{0,H/V}$ map and

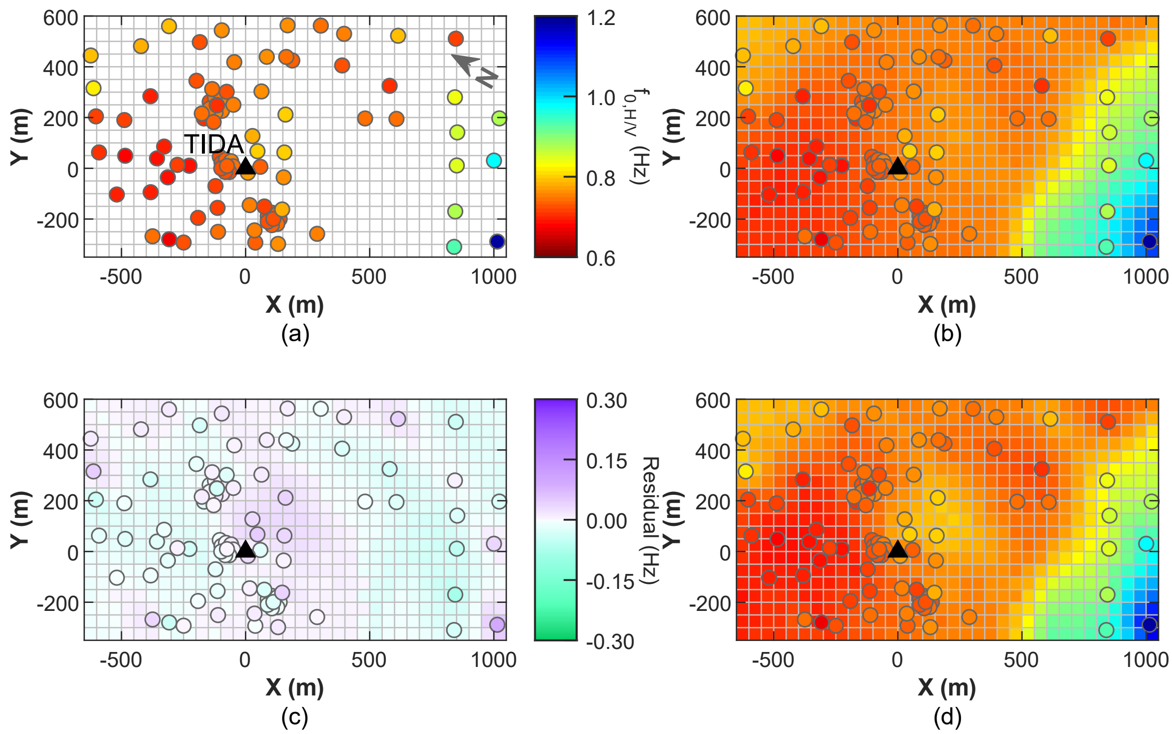

Figure 5. Uniformly estimated $f_{0,H/V}$ map at TIDA. Shown on a 50-m grid are: (a) 97 measured $f_{0,H/V}$ values, (b) $f_{0,H/V}$ trend obtained from a moving window average of the measurements, (c) uniformly estimated $f_{0,H/V}$ residual map obtained from kriging on the residuals (shown using circles), which are calculated by subtracting the trend from the $f_{0,H/V}$ measurements, and (d) the final uniformly estimated $f_{0,H/V}$ map obtained from summing the trend map (i.e., b) and the kriged residual map (i.e., c). The measured $f_{0,H/V}$ values are presented in (b) and (d) for comparison.

the H/V measurement nearest to the location of the measured Vs profile are used to calculate a uniform scaling factor map. Finally, the uniformly calculated scaling factor map and the measured Vs profile are used to build a pseudo-3D Vs model on the same uniform grid by scaling the layer thicknesses of the measured Vs profile.

Uniformly Estimated $f_{0,H/V}$ Maps

The first step of the H/V geostatistical approach (Figure 2) requires uniformly mapping $f_{0,H/V}$ over an area of interest using the irregularly sampled H/V measurements; this is achieved herein using the kriging with a trend model approach (Hengl et al., 2004; Isaaks and Srivastava, 1989). The kriging with a trend model approach is illustrated for the TIDA and DPDA sites in Figures 5 and 6, respectively. Presented are: (a) measured $f_{0,H/V}$ values, (b) $f_{0,H/V}$ trend map, (c) $f_{0,H/V}$ residual map, and (d) the final uniformly estimated $f_{0,H/V}$ map. The $f_{0,H/V}$ trend map at TIDA (Figure 5b), which is a moving window average of the measurements (Figure 5a), is comparable to the final uniformly estimated $f_{0,H/V}$ map (Figure 5d). Hence, adding the trend map and the residual map (Figure 5c) obtained from kriging on the residuals (i.e., the difference between the measurements and the trend) only causes minimal improvements in the final $f_{0,H/V}$ map by ± 0.1 Hz at most. This is mainly due to the relatively dense and uniform H/V spatial sampling at TIDA.

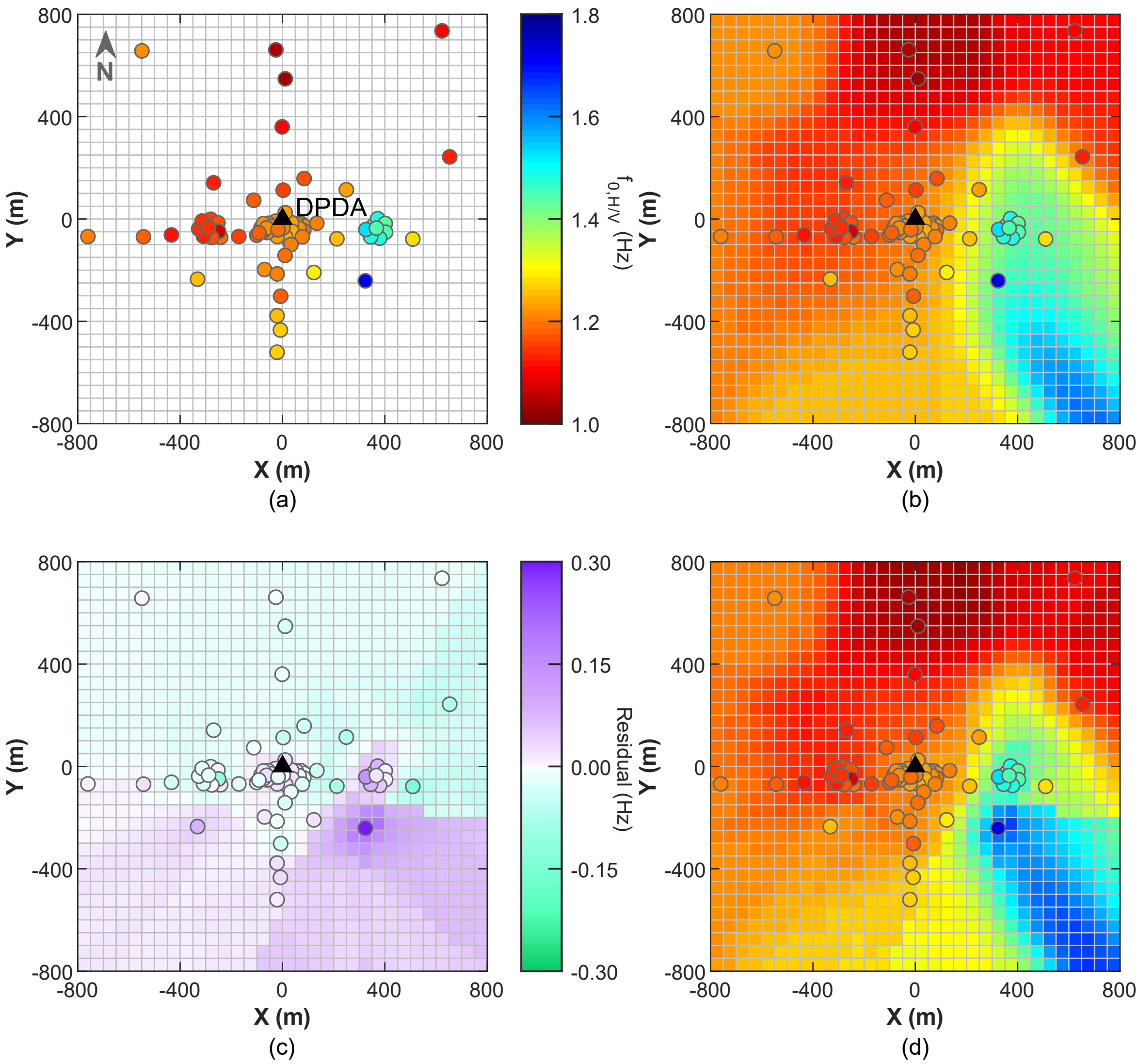

Figure 6. Uniformly estimated $f_{0,H/V}$ map at DPDA. Shown on a 50-m grid are: (a) 96 measured $f_{0,H/V}$ values, (b) $f_{0,H/V}$ trend obtained from a moving window average of the measurements, (c) uniformly estimated $f_{0,H/V}$ residual map obtained from kriging on the residuals (shown using circles), which are calculated by subtracting the trend from the $f_{0,H/V}$ measurements, and (d) the final uniformly estimated $f_{0,H/V}$ map obtained from summing the trend map (i.e., b) and the kriged residual map (i.e., c). The measured $f_{0,H/V}$ values are presented in (b) and (d) for comparison.

On the other hand, due to the more spatially irregular $f_{0,H/V}$ measurements at DPDA, performing kriging on the residuals (Figure 6c) causes more significant improvement in the estimated map. It is clear that by adding the kriged residual map to the trend, the resulting uniformly estimated $f_{0,H/V}$ map (Figure 6d) better matches the measured values compared to the trend map alone (Figure 6b). This is most evident in the south-east quadrant where the final uniformly estimated map is improved by up to 0.3 Hz. Thus, depending on the site and the spatial distribution of the measurements, different spatial estimation techniques could be used to obtain a uniformly estimated $f_{0,H/V}$ map. Simple modeling approaches, such as a moving window average of the measurements, could be potentially used when the measurements are relatively dense and

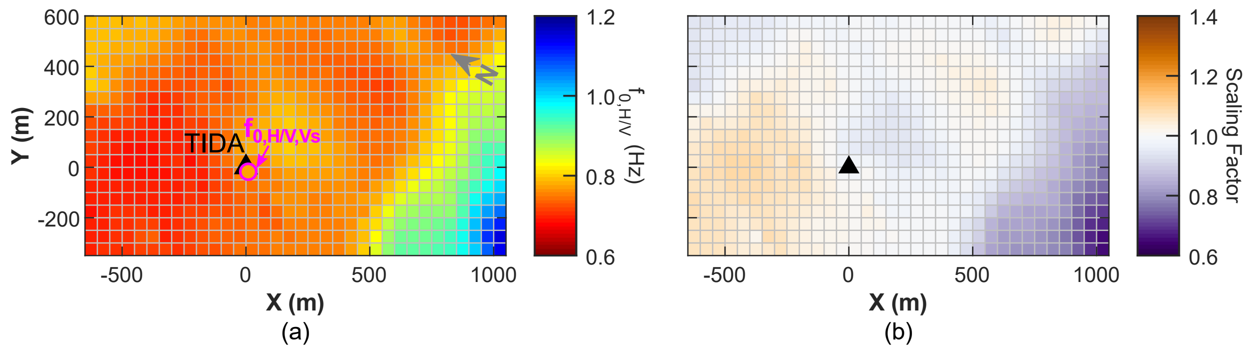

Figure 7. Uniformly calculated S_{f_0} map required to scale the layer thicknesses of the measured Vs profile to match the estimated $f_{0,H/V}$ map at the TIDA site. Shown on a 50-m grid are: (a) the uniformly estimated $f_{0,H/V}$ map obtained from the kriging with a trend model approach (i.e., Figure 5d), and (b) the uniformly calculated S_{f_0} map obtained from dividing the $f_{0,H/V}$ measurement nearest to the TIDA (also location of Vs measurement) by the estimated $f_{0,H/V}$ value of each cell (i.e., a). Note that the $f_{0,H/V}$ measurement nearest to the TIDA is highlighted using magenta in (a).

uniform enough to capture changes in $f_{0,H/V}$ (e.g., TIDA), whereas more advanced approaches, such as kriging, could be needed when the measurements are sparse and spatially irregular (e.g., DPDA). However, regardless of the distribution of the measurements, kriging is expected to provide the estimated $f_{0,H/V}$ map that best fits the measurements since it is a generalized least-squares regression.

Uniformly Calculated S_{f_0} Maps

After estimating $f_{0,H/V}$ over a uniform grid, the second step requires dividing the H/V measurement closest to the location of the measured Vs profile (i.e., $f_{0,H/V,Vs}$) by the uniformly estimated $f_{0,H/V}$ map to obtain a scaling factor map. The scaling factor maps for the TIDA and DPDA sites are presented in Figures 7 and 8, respectively. Presented are: (a) the uniformly estimated $f_{0,H/V}$ maps, and (b) the uniformly calculated S_{f_0} maps; the $f_{0,H/V,Vs}$ values used in the calculations are highlighted using magenta in (a). The $f_{0,H/V,Vs}$ at the TIDA is equal to 0.78 Hz, resulting in S_{f_0} values ranging between 0.65 and 1.10 (Figure 7b). The estimated $f_{0,H/V}$ map (Figure 7a) shows relatively minimal variability in $f_{0,H/V}$ up to around 500 m away from the downhole array site in all directions, resulting in scaling factors close to 1.0 near the TIDA boreholes. However, the distribution of S_{f_0} at TIDA appears to be negatively skewed (i.e., skewed to low S_{f_0}) due to the higher $f_{0,H/V}$ values near the causeway to YBI (refer to Figure 4a). Since the layer thicknesses of the measured Vs profile will be multiplied by the negatively skewed scaling factors, then we expect the scaled Vs profiles at TIDA to be also skewed toward shallower bedrock.

As for DPDA, the $f_{0,H/V,Vs}$ is equal to 1.24 Hz, resulting in S_{f_0} values ranging between 0.75 and 1.20 (Figure 8b). The variability in the uniformly estimated $f_{0,H/V}$ map (Figure 8a) is relatively significant, resulting in S_{f_0} that deviate to values both greater and less than 1.0 in as little as 300 m away from the DPDA boreholes. However, the distribution of S_{f_0} at DPDA appears to be relatively symmetric, with nearly equal number of cells having scaling factors that deviate by approximately $\pm$ 0.3 from 1.0. Thus, we expect the scaled Vs profiles at DPDA to also be relatively symmetric

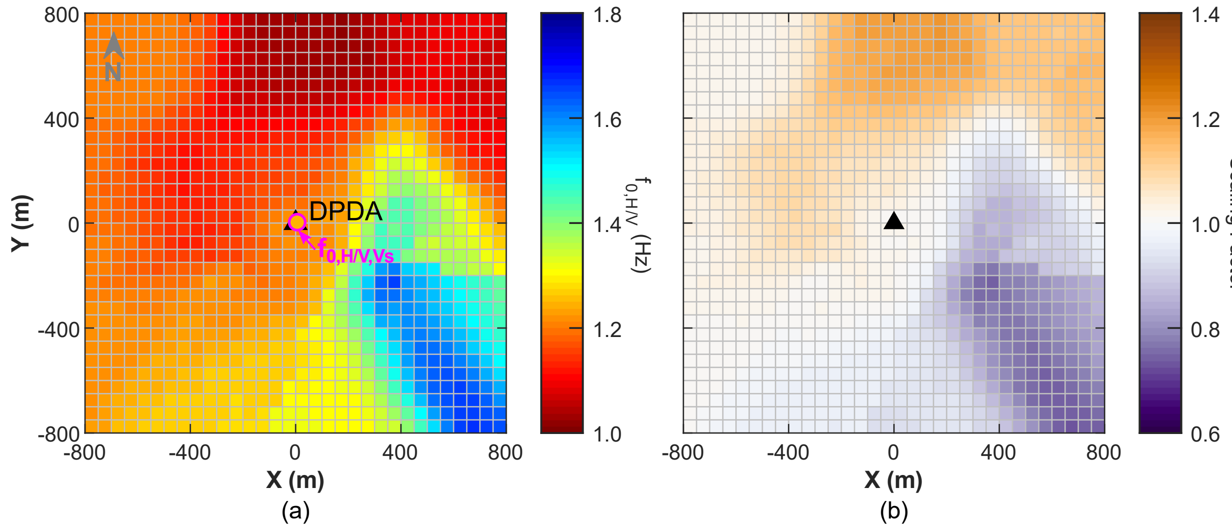

Figure 8. Uniformly calculated S_{f_0} map required to scale the layer thicknesses of the measured Vs profile to match the estimated $f_{0,H/V}$ map at the DPDA site. Shown on a 50-m grid are: (a) the uniformly estimated $f_{0,H/V}$ map obtained from the kriging with a trend model approach (i.e., Figure 6d), and (b) the uniformly calculated S_{f_0} map obtained from dividing the $f_{0,H/V}$ measurement nearest to the DPDA (also location of Vs measurement) by the estimated $f_{0,H/V}$ value of each cell (i.e., a). Note that the $f_{0,H/V}$ measurement nearest to the DPDA is highlighted using magenta in (a).

about the measured Vs regarding depth to glacial till. This is in contrast to TIDA, where the spatial variability in S_{f_0} is less significant in terms of its magnitude but skewed to low values.

Pseudo-3D Vs Models

To finally build the pseudo-3D Vs models, Vs profiles are developed on the same uniform grid by simply multiplying the layer thicknesses of the measured Vs profile by the S_{f_0} of each cell. The resulting pseudo-3D Vs model at the TIDA site is shown in Figure 9. Presented are: (a) the uniformly estimated $f_{0,H/V}$ map, (b) the scaled Vs profiles shown in 1D, but color coded to match values in the uniformly estimated $f_{0,H/V}$ map, (c) two 2D Vs cross sections, and (d) a 3D view of the 2D Vs cross sections. The locations of the cross sections are shown in Figure 9a. A total of 646 50-m cells were considered in the analysis at TIDA, resulting in a pseudo-3D model with approximate surface dimensions of 1.6 km by 1.0 km.

As expected, the relatively uniform scaling factors of 1.0 near the TIDA boreholes (Figure 7b), result in scaled Vs profiles (Figure 9b) that are mostly comparable to the measured one. It is also clear that the variability is skewed toward a shallower soil-rock interface (i.e., higher $f_{0,H/V}$ values) near the causeway to YBI in the south, which implies stiffer subsurface conditions; this is evident in cross section A-A’, which as shown in Figure 9a, extends near the causeway to YBI. The minimal spatial variability close to the TIDA site is consistent with available geologic cross sections, which show that the near subsurface in that area is horizontally stratified (Papadopulos and Eliahu, 2009). The geologic cross sections, however, do not extend close to YBI. Nevertheless, as discussed earlier, shallower bedrock is expected in the south direction as the rocks of the Franciscan Formation slope upward and ultimately outcrop on YBI.

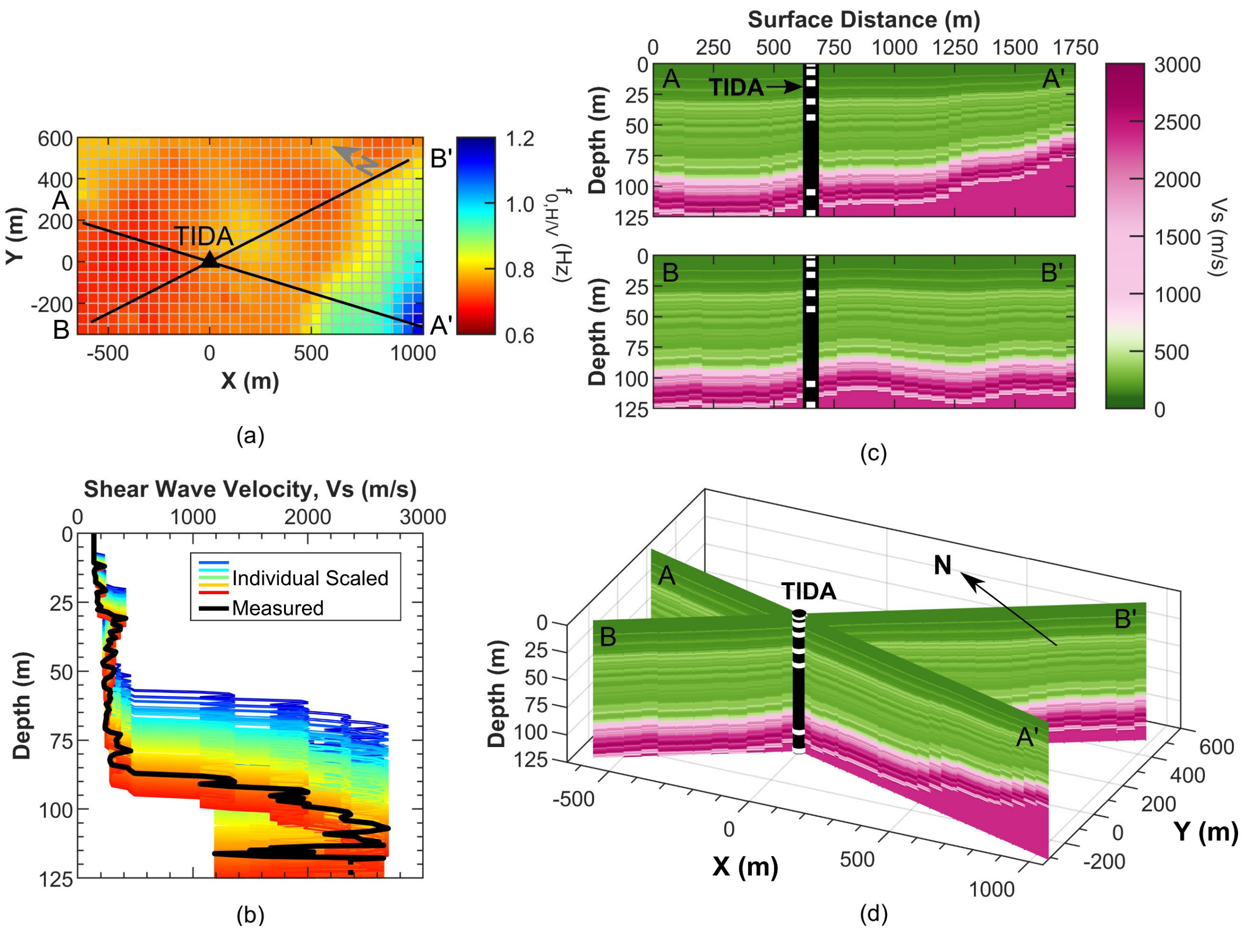

Figure 9. Pseudo-3D Vs model developed using the H/V geostatistical approach at the TIDA site. Shown are: (a) the uniformly estimated $f_{0,H/V}$ map, (b) 1D representation of the spatially variable V_S profiles calculated from the measured profile and the scaling factors (Figure 7b), (c) 2D Vs cross sections A-A' and B-B', and (d) 3D fence diagram of the 2D Vs cross sections. Note that the scaled 1D Vs profiles in (b) are colored by the $f_{0,H/V}$ values of their corresponding cells shown in (a). The borehole array and triaxial accelerometer sensor depths are shown in black and white, respectively, in both (c) and (d).

The pseudo-3D Vs model at the DPDA site is demonstrated in Figure 10. A total of 1,024 50-m cells were considered in the analysis, resulting in a pseudo-3D model with a footprint of 1.6 km by 1.6 km. The scaled Vs profiles (Figure 10b) mirror many features observed in the $f_{0,H/V}$ map (Figure 10a) and S_{f_0} map (Figure 8b). As expected, the highly variable $f_{0,H/V}$ and S_{f_0} maps near the DPDA boreholes result in many scaled Vs profiles with both shallower or deeper glacial till. This variability, while significant, is relatively symmetric about the measured Vs profile. The lower $f_{0,H/V}$ values in the north result in scaling factors above 1.0, and consequently, deeper glacial till. This is evident in the scaled Vs profiles shown in dark red (Figure 10b) and in cross section B-B'. Conversely, the higher $f_{0,H/V}$ values in the south-east quadrant result in scaling factors below 1.0, and consequently, shallower glacial till, which is evident in the scaled Vs profiles shown in blue (Figure 10b) and in cross section A-A'. The pattern of the Vs variability is in good agreement with several geologic cross sections around the site, which show deeper and shallower glacial till in the north and east directions, respectively (Combellick, 1999).

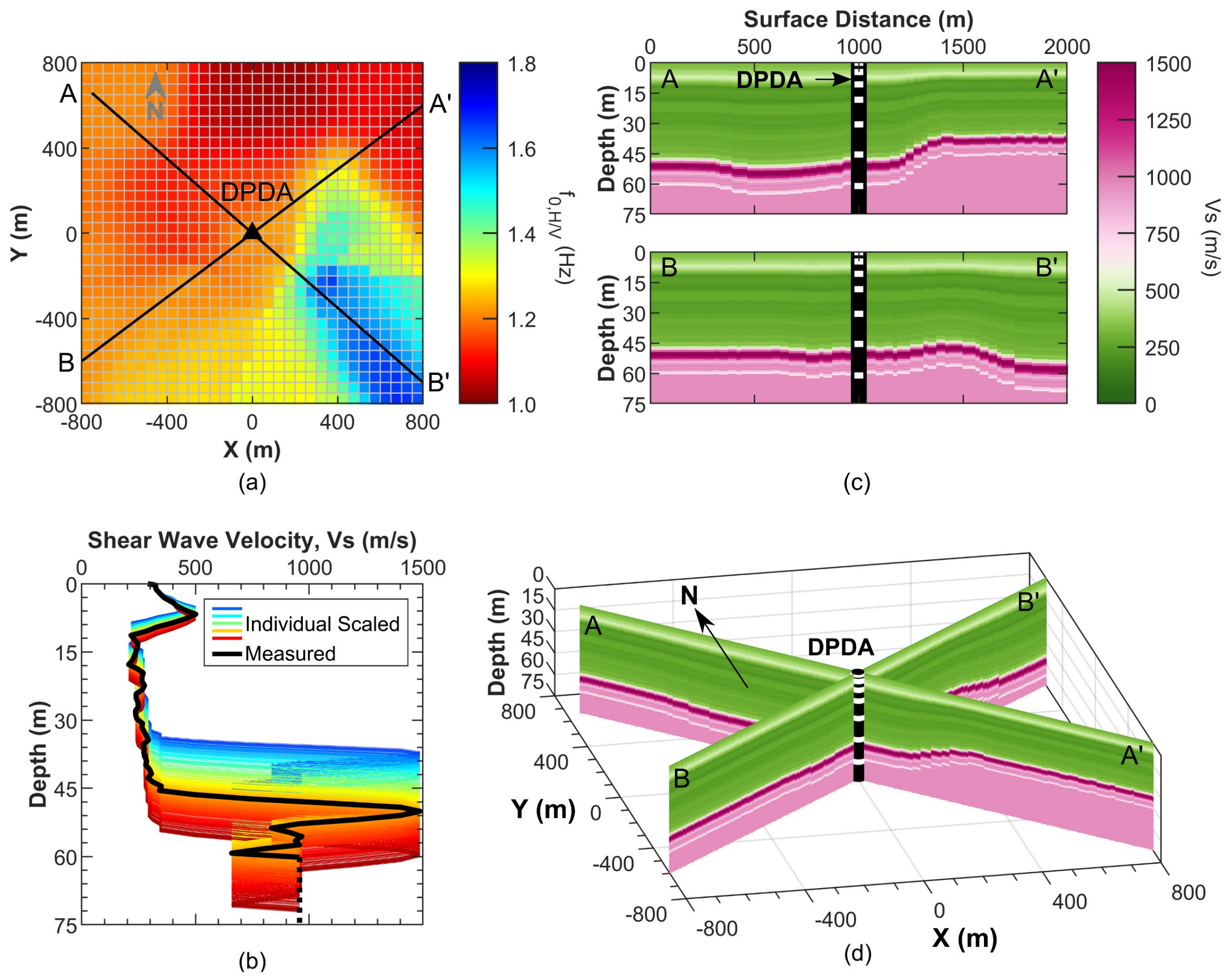

Figure 10. Pseudo-3D Vs model developed using the H/V geostatistical approach at the DPDA site. Shown are: (a) the uniformly estimated $f_{0,H/V}$ map, (b) 1D representation of the spatially variable V_S profiles calculated from the measured profile and the scaling factors (Figure 8b), (c) 2D Vs cross sections A-A' and B-B', and (d) 3D fence diagram of the 2D Vs cross sections. Note that the scaled 1D Vs profiles in (b) are colored by the $f_{0,H/V}$ values of their corresponding cells shown in (a). The borehole array and triaxial accelerometer sensor depths are shown in black and white, respectively, in both (c) and (d).

Discussion

We have observed that the TIDA site has low variability that is skewed to shallower bedrock toward the south, near the causeway to YBI, whereas the DPDA site has high Vs variability but which is relatively symmetric about the measured Vs profile near the downhole array site. Such variability could not be represented by purely stochastic models based on generic parameters derived for other sites or simply assumed. This underscores the importance of building Vs models based on in-situ measurements to ensure proper incorporation of site-specific spatial variability in GRAs. The aforementioned evaluation of the site-specific variability at each site was qualitative and herein, we present quantitative measures of the spatial variability at each site. We believe that the Vs models should reflect both the magnitude and skewness of the spatial variability. The magnitude is the extent of the variability and can be quantified using the standard deviation. The skewness should indicate whether variability is favored in a certain direction, such as having mostly stiffer or softer conditions in a certain area or direction around the site, and is quantified using the sample skewness.

The descriptive statistics of the site-specific spatial variability (i.e., standard deviation and skewness) are evaluated herein for the uniformly calculated S_{f_0} values. We choose S_{f_0} instead of $f_{0,H/V}$ because the former values are normalized; this ensures that the difference in magnitude of $f_{0,H/V}$ between the sites does not affect the results. While the descriptive statistics can be calculated at each site over the entire grid, we present the results as a function of several discrete incorporated areas. This allows us to compare the variability at both sites across similar incorporated areas and eventually provide insights on the area likely influencing site response. We incrementally increase the area surrounding the downhole array site by one cell (i.e., by 50 m) in each of the four directions (north, south, east, and west) and calculate the standard deviation and skewness for each incorporated area. For TIDA, in which the geometry of the map is asymmetric, we keep on increasing the incorporated area in the directions that can be extended, until covering the full map.

Magnitude of Spatial Variability

We calculate the lognormal standard deviation in S_{f_0} ($\sigma_{\ln S_{f0}}$) since lognormal distributions are common in geotechnical earthquake applications; this also allows for a seamless transition between the standard deviation of S_{f_0}, $f_{0,H/V}$, and that of depth to rock (z_{rock}), as discussed later in this section. The $\sigma_{\ln S_{f0}}$ comparison is presented in Figure 11a. Additionally, for clarity, we highlight different areas in Figure 11a; those areas are outlined in the uniformly calculated S_{f_0} maps at TIDA and DPDA in Figures 11c and 11d, respectively. While the sites have comparable variability at small incorporated areas, DPDA has an increased $\sigma_{\ln S_{f0}}$ beyond an incorporated area of 400 m x 400 m (i.e., the area highlighted in teal; 0.16 km^2). This observation is in line with Tao and Rathje (2019), who hypothesized that the DPDA site is more variable than TIDA based on geology and results from 1D GRAs. However, in this paper, we additionally highlight the need to identify an area of interest, as DPDA is more variable only after a certain area is incorporated. This issue is addressed in Hallal and Cox (2020), in which the effects of the incorporated area on the site response predictions are examined.

The evaluation of the standard deviation of S_{f_0} in logarithmic space results in an interesting correspondence between $\sigma_{\ln S_{f0}}$ and that of $f_{0,H/V}$ ($\sigma_{\ln f_{0,H/V}}$) and depth to rock ($\sigma_{\ln Z_{rock}}$). The lognormal standard deviation depth to rock is commonly used as an input parameter in Vs randomization approaches to estimate the variation in the depth to bedrock. Following Equation 2 of the H/V geostatistical approach, and by replacing the thickness of the soil column above bedrock (H) by the depth to bedrock (z_{rock}), the relation shown in Equation 3 can be obtained.

$$S_{f_0} = \frac{z_{rock}}{z_{rock,Vs}} \rightarrow ln(z_{rock}) = ln(z_{rock,Vs}) + ln(S_{f_0}) \tag{3}$$

Then, by evaluating the variance of the left- and right-hand side of Equation 3, we can easily show that the variance in z_{rock} is equal to that in S_{f_0} in logarithmic space, as shown in Equation 4. This is true because the bedrock depth of the measured Vs profile ($z_{rock,Vs}$) is a constant and does not affect the value of the variance. Hence, by taking the square root of the variance, we can prove

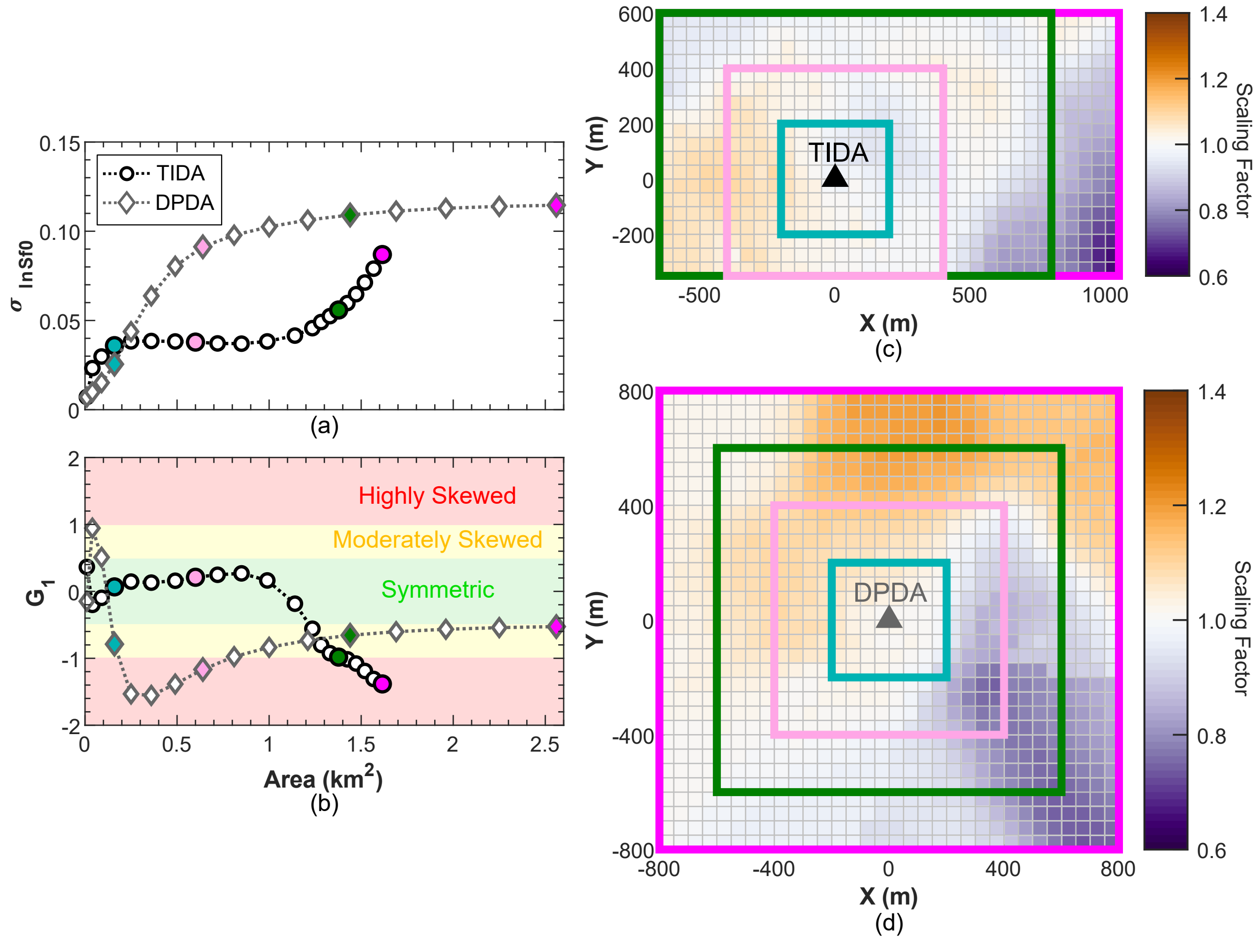

Figure 11. Effect of varying the incorporated spatial area in the uniformly calculated S_{f_0} map on: (a) the lognormal standard deviation in S_{f_0} ($\sigma_{lnS_{f0}}$), and (b) the sample skewness (G_1) of S_{f_0}. (c & d) The uniformly calculated S_{f_0} map at TIDA and DPDA, respectively, showing the selected areas whose results are highlighted in (a) and (b) using the same colors. Note that $\sigma_{lnS_{f0}}$ is equal to the standard deviation of $f_{0,H/V}$ in logarithmic space ($\sigma_{lnf_{0,H/V}}$).

that $\sigma_{lnS_{f0}} = \sigma_{lnZrock}$. The same logic can be used to show that $\sigma_{lnS_{f0}} = \sigma_{lnf_{0,H/V}}$. Thus, without having to calculate scaling factors and just by calculating $\sigma_{lnf_{0,H/V}}$, engineers can obtain an estimate of the site-specific $\sigma_{lnZrock}$ and consequently, use better-informed parameters when applying Vs randomization for GRAs. However, this is only true under the assumptions of the H/V geostatistical approach, wherein the layer thicknesses and depth to the major impedance contrast are assumed to be primarily controlling the change in $f_{0,H/V}$.

$$Var[ln(z_{rock})] = Var\left[ln\left(z_{rock,Vs}\right) + ln\left(S_{f_0}\right)\right] = Var\left[ln\left(S_{f_0}\right)\right] \rightarrow \sigma_{lnZ_{rock}} = \sigma_{lnS_{f_0}} \tag{4}$$

Skewness of Spatial Variability

Another important descriptive statistic of the site-specific spatial variability is its skewness. While the standard deviation quantifies the extent of the variability, it does not provide any information on the direction of this variability, which as shown in Hallal and Cox (2020), affects the site response. To quantify this direction, we use the sample skewness (G_1) as shown in Equation 5 (Joanes and Gill, 1998). In this equation, n is the total number of cells in the incorporated area.

$$G_1 = \sqrt{\frac{n(n-1)}{n-2}} \frac{\frac{1}{n}\sum_{i=1}^{n}\left(S_{f_{0,i}} - \overline{S_{f_0}}\right)^3}{\left(\sqrt{\frac{1}{n}\sum_{i=1}^{n}\left(S_{f_{0,i}} - \overline{S_{f_0}}\right)^2}\right)^3} \tag{5}$$

The variation of the skewness as a function of the incorporated area at both sites is presented in Figure 11b. Generally, a G_1 value of zero indicates a symmetric distribution, whereas a negative value implies skewness to low values, and vice versa. We observe that the distribution of S_{f_0} at TIDA is approximately symmetric up to an area of approximately 1,400 m x 1,000 m (i.e., the area highlighted in dark green; approximately 1.4 km^2), beyond which it starts to become highly negatively skewed, whereas DPDA is mostly negatively skewed but gradually becomes less skewed beyond an area of 800 m x 800 m (i.e., the area highlighted in light pink; 0.64 km^2). Based on the G_1 boundaries set by Bulmer (1979) for symmetric, moderately skewed, and highly skewed distributions, which are highlighted in Figure 11b using green, yellow, and red shading, respectively, the distribution of S_{f_0} when incorporating the full area at TIDA is considered to be highly skewed ($G_1 < -1$) whereas that at DPDA is at the boundary between symmetric and moderately skewed ($G_1 \approx -0.5$). Again, the change of the skewness with area illustrates the importance of specifying an area of interest over which the spatial variability needs to be modeled. It also highlights the need to figure out the spatial area that impacts site response at any given location. The areas influencing recorded site response at TIDA and DPDA are investigated in the companion paper by Hallal and Cox (2020).

Conclusions

Accounting for spatial variability in subsurface conditions is of paramount importance for seismic analysis, design, and risk assessment. While this paper is not the first to recognize the need to implement an approach that could be tailored to account for site-specific spatial variability in GRAs, no study we are aware of attempts to do so using simple, cost-effective site measurements that could be feasibly obtained. This paper proposes a method for building a pseudo-3D Vs model based on a geostatistical framework of H/V measurements that can be used to incorporate spatial variability into 1D, 2D, and 3D GRAs. The new framework utilizes easily attained measurements that provide valuable information about the variation of properties known to strongly impact site-specific wave propagation, does not require the assumption of a probabilistic model to map the spatial variability with tens to hundreds of realizations, and enables the construction of a realistic pseudo-3D Vs model.

The scaled Vs profiles built using the H/V geostatistical approach are expected to be a more realistic representation of the actual subsurface conditions than purely stochastic models, which generally use input parameters derived for other sites or simply assumed. The rationale behind this argument is that a unique spatial variability exists for each site, meaning that calculated parameters based on relationships derived for other sites in the literature may not represent the actual site properties. Additionally, the subsurface properties are spatially correlated rather than completely random, and this spatial correlation also varies from site to site. The H/V approach addresses both of these issues by integrating site-specific H/V measurements, which are dependent on subsurface conditions, with geostatistical tools that can model the site-specific spatial correlation of the subsurface properties. Additionally, the approach utilizes the experimental site signature, which allows for Vs uncertainty to be accounted for in a rational manner.

While the implementation of the H/V geostatistical approach at the two case study sites presented herein was each based on approximately 100 H/V measurements, the approach could certainly be implemented with fewer measurement locations. Even so, the H/V data was collected easily at each site in less than two full workdays by crews of 4-5 people using 10 seismometers. This is less than the amount of time dedicated to typical geotechnical site characterizations on even routine projects. Furthermore, this testing could have been performed faster, as many of the H/V measurements were clustered in arrays as part of surface wave MAM testing, which are not needed for implementing the H/V approach. For future applications, the H/V measurements should be relatively uniformly distributed across the area of interest, with good azimuthal coverage where possible.

The proposed methodology for building psuedo-3D Vs models aims to achieve the ultimate goal of improving the modeling of site response in engineering practice. The approach attempts to account for realistic Vs spatial variability in a meaningful way using site-specific measurements that are relevant to site response. Furthermore, as the same pseudo-3D Vs models can be incorporated in 1D, 2D, and 3D GRAs, this allows for future research on the appropriate/necessary dimensionality of GRAs at different sites. In addition, the pseudo-3D Vs model can provide valuable information on the subsurface structure for applications such as estimating the depth to significant Vs horizons and lognormal standard deviation on depth to rock for use in ground motion prediction equations and Vs randomization. While the accuracy of the generated Vs models was evaluated only in comparison to geologic information, a further validation and comparison of the predicted and observed ground motions at TIDA and DPDA using 1D GRAs that incorporate the pseudo-3D Vs models are discussed in the accompanying paper by Hallal and Cox (2020).

Acknowledgements

The H/V data from TIDA and DPDA were collected with funding from Pacific Gas and Electric (PG&E). However, any opinions, findings, conclusions, or recommendations expressed in this paper are those of the authors and do not necessarily reflect the views of PG&E. We would like to thank Mr. Joseph Vantassel and Mr. Michael Yust for their help in planning and collecting the H/V data at TIDA and DPDA, and Dr. Albert Kottke, Dr. David Teague, and Dr. Krishna Kumar for their help in collecting the H/V data at TIDA.

References

Afshari K and Stewart JP (2019) Insights from california vertical arrays on the effectiveness of ground response analysis with alternative damping models. *Bulletin of the Seismological Society of America* 109(4): 1250–1264. DOI: 10.1785/0120180292.

Albarello D and Lunedei E (2013) Combining horizontal ambient vibration components for H/V spectral ratio estimates. *Geophysical Journal International* 194(2): 936–951. DOI: 10.1093/gji/ggt130.

Assimaki D, Pecker A, Popescu R, et al. (2003) Effects of spatial variability of soil properties on surface ground motion. *Journal of Earthquake Engineering* 7: 1–44. DOI: 10.1080/13632460309350472.

Badal J, Dutta U, Serón F, et al. (2004) Three-dimensional imaging of shear wave velocity in the uppermost 30 m of the soil column in Anchorage, Alaska. *Geophysical Journal International* 158(3): 983–997. DOI: 10.1111/j.1365-246X.2004.02327.x.

Bard PY and SESAME-Team (2004) *Guidelines for the implementation of the H/V spectral ratio technique on ambient vibrations-measurements, processing and interpretations*. SESAME European Research Project No. EVG1-CT-2000-00026. Brussels, Belgium: European Commission.

Bonnefoy-Claudet S, Cotton F and Bard PY (2006) The nature of noise wavefield and its applications for site effects studies. A literature review. *Earth-Science Reviews* 79(3–4): 205–227. DOI: 10.1016/j.earscirev.2006.07.004.

Bulmer MG (1979) *Principles of Statistics*. New York, NY: Dover Publications.

Chen H, Ni S, Chu R, et al. (2018) Influence of the off-great-circle propagation of Rayleigh waves on event-based surface wave tomography in Northeast China. *Geophysical Journal International* 214(2): 1105–1124. DOI: 10.1093/GJI/GGY185.

Cheng T, Cox BR, Vantassel JP, et al. (2020) A Statistical Approach to Account for Azimuthal Variability in Single-Station HVSR Measurements. *Geophysical Journal International*. In Review.

Combellick RA (1999) *Simplified Geologic Map and Cross Sections of Central and East Anchorage , Alaska*. Preliminary Interpretive Rep. No. 1999-1. Fairbanks, AK: Alaska Division of Geological & Geophysical Surveys. DOI: 10.14509/2243.

Cox BR, Cheng T, Vantassel JP, et al. (2020) A statistical representation and frequency-domain window-rejection algorithm for single-station HVSR measurements. *Geophysical Journal International* 221(3): 2170–2183. DOI: 10.1093/gji/ggaa119.

de Alba P, Benoit J, Pass DG, et al. (1994) *Deep instrumentation array at the Treasure Island Naval Station*. US Geological Survey Professional Paper 1551 A: 155–168. Washington, DC: USGS. DOI: 10.1016/0148-9062(95)99406-n.

de la Torre C, McGann C, Bradely B, et al. (2019) 3D Sesimic Site Response with Soil Heterogeneity and Wave Scattering in OpenSees. In: *Proceedings of the 1st Eurasian Conference on Opensees: Opensees Days Eurasia*, Hong Kong SAR, China, 20-21 June, 2019.

Endrun B (2011) Love wave contribution to the ambient vibration H/V amplitude peak observed with array measurements. *Journal of Seismology* 15(3): 443–472. DOI: 10.1007/s10950-010-9191-x.

Fäh D, Kind F and Giardini D (2001) A theoretical investigation of average HIV ratios. *Geophysical Journal International* 145(2): 535–549. DOI: 10.1046/j.0956-540X.2001.01406.x.

Fäh D, Kind F and Giardini D (2003) Inversion of local S-wave velocity structures from average H/V ratios, and their use for the estimation of site-effects. *Journal of Seismology* 7(4): 449–467. DOI: 10.1023/B:JOSE.0000005712.86058.42.

Foti S, Parolai S, Albarello D, et al. (2011) Application of Surface-Wave Methods for Seismic Site

Characterization. *Surveys in Geophysics* 32(6): 777–825. DOI: 10.1007/s10712-011-9134-2.

Gibbs JF, Fumal TE, Boore DM, et al. (1992) *Seismic velocities and geologic logs from borehole measurements at seven strong-motion stations that recorded the 1989 Loma Prieta, California, earthquake*. U.S. Geological Survey Open-File Report 92-287. Menlo Park, CA: USGS.

Graizer V and Shakal A (2004) Analysis of CSMIP strong-motion geotechnical array recordings. In: *International Workshop for Site Selection, Installation, and Operation of Geotechnical Strong-Motion Arrays*, Sacramento, CA.

Griffiths SC, Cox BR, Rathje EM, et al. (2016a) Mapping dispersion misfit and uncertainty in Vs profiles to variability in site response estimates. *Journal of Geotechnical and Geoenvironmental Engineering* 142(11). DOI: 10.1061/(ASCE)GT.1943-5606.0001553.

Griffiths SC, Cox BR, Rathje EM, et al. (2016b) Surface-wave dispersion approach for evaluating statistical models that account for shear-wave velocity uncertainty. *Journal of Geotechnical and Geoenvironmental Engineering* 142(11). DOI: 10.1061/(ASCE)GT.1943-5606.0001552.

Haghshenas E, Bard PY, Theodulidis N, et al. (2008) Empirical evaluation of microtremor H/V spectral ratio. *Bulletin of Earthquake Engineering* 6(1): 75–108. DOI: 10.1007/s10518-007-9058-x.

Hallal MM and Cox BR (2020) An H/V Geostatistical Approach for Building Pseudo-3D Vs Models to Account for Spatial Variability in Ground Response Analyses II: Application to 1D Analyses at Two Downhole Array Sites. engrXiv. Available from: engrxiv.org/4nrs6. DOI: 10.31224/osf.io/4nrs6.

Hengl T, Heuvelink GBM and Stein A (2004) A generic framework for spatial prediction of soil variables based on regression-kriging. *Geoderma* 120(1–2): 75–93. DOI: 10.1016/j.geoderma.2003.08.018.

Hobiger M, Cornou C, Wathelet M, et al. (2013) Ground structure imaging by inversions of Rayleigh wave ellipticity: Sensitivity analysis and application to European strong-motion sites. *Geophysical Journal International* 192(1): 207–229. DOI: 10.1093/gji/ggs005.

Isaaks EH and Srivastava RM (1989) *An Introduction to Applied Geostatistics*. New York: Oxford University Press.

Ismail A, Brett Denny F and Metwaly M (2014) Comparing continuous profiles from MASW and shear-wave reflection seismic methods. *Journal of Applied Geophysics* 105: 67–77. DOI: 10.1016/j.jappgeo.2014.03.007.

Joanes DN and Gill CA (1998) Comparing measures of sample skewness and kurtosis. *Journal of the Royal Statistical Society Series D: The Statistician* 47(1): 183–189. DOI: 10.1111/1467-9884.00122.

Kaklamanos J and Bradley BA (2018) Challenges in predicting seismic site response with 1d analyses: Conclusions from 114 kik-net vertical seismometer arrays. *Bulletin of the Seismological Society of America* 108(5): 2816–2838. DOI: 10.1785/0120180062.

Kaklamanos J, Bradley BA, Thompson EM, et al. (2013) Critical parameters affecting bias and variability in site-response analyses using KiK-net downhole array data. *Bulletin of the Seismological Society of America* 103(3): 1733–1749. DOI: 10.1785/0120120166.

Kaklamanos J, Baise LG, Thompson EM, et al. (2015) Comparison of 1D linear, equivalent-linear, and nonlinear site response models at six KiK-net validation sites. *Soil Dynamics and Earthquake Engineering* 69: 207–219. DOI: 10.1016/j.soildyn.2014.10.016.

Kallivokas LF, Fathi A, Kucukcoban S, et al. (2013) Site characterization using full waveform inversion. *Soil Dynamics and Earthquake Engineering* 47: 62–82. DOI: 10.1016/j.soildyn.2012.12.012.

Lachet C and Bard PY (1994) Numerical and Theoretical Investigations on the Possibilities and Limitations of Nakamura's Technique. *Journal of Physics of the Earth* 42(5): 377–397. DOI: 10.4294/jpe1952.42.377.

Lermo J and Chavez-Garcia FJ (1993) Site effect evaluation using spectral ratios with only one station. *Bulletin - Seismological Society of America* 83(5): 1574–1594.

Luo Y, Xia J, Liu J, et al. (2008) Generation of a pseudo-2D shear-wave velocity section by inversion of a series of 1D dispersion curves. *Journal of Applied Geophysics* 64(3–4): 115–124. DOI: 10.1016/j.jappgeo.2008.01.003.

Mahvelati S and Coe JT (2017) The use of two dimensional (2D) Multichannel Analysis of Surface Waves (MASW) testing to evaluate the geometry of an unknown bridge foundation. In: *Geotechnical Special Publication*, 2017, pp. 657–666. DOI: 10.1061/9780784480441.069.

Mi B, Xia J, Shen C, et al. (2017) Horizontal resolution of multichannel analysis of surface waves. *Geophysics* 82(3): EN51–EN66. DOI: 10.1190/GEO2016-0202.1.

Nakamura Y (1989) Method for dynamic characteristics estimation of subsurface using microtremor on the ground surface. *Railway Technical Research Institute* 30(1): 25–33.

Nath SK, Chatterjee D, Biswas NN, et al. (1997) Correlation study of shear wave velocity in near surface geological formations in Anchorage, Alaska. *Earthquake Spectra* 13(1): 55–75. DOI: 10.1193/1.1585932.

Nogoshi M and Igarashi T (1971) On the Amplitude Characteristics of Microtremor (Part 2). *Zisin (Journal of the Seismological Society of Japan. 2nd ser.)* 24(1): 26–40. DOI: 10.4294/zisin1948.24.1_26.

Nour A, Slimani A, Laouami N, et al. (2003) Finite element model for the probabilistic seismic response of heterogeneous soil profile. *Soil Dynamics and Earthquake Engineering* 23(5): 331–348. DOI: 10.1016/S0267-7261(03)00036-8.

Pan Y, Schaneng S, Steinweg T, et al. (2018) Estimating S-wave velocities from 3D 9-component shallow seismic data using local Rayleigh-wave dispersion curves – A field study. *Journal of Applied Geophysics* 159: 532–539. DOI: 10.1016/j.jappgeo.2018.09.037.

Pan Y, Gao L and Bohlen T (2019) High-Resolution Characterization of Near-Surface Structures by Surface-Wave Inversions: From Dispersion Curve to Full Waveform. *Surveys in Geophysics*. DOI: 10.1007/s10712-019-09508-0.

Papadopulos S and Eliahu U (2009) *Geotechnical Conceptual Design Report – Treasure Island, San Francisco, CA*. ENGEO.

Park CB (2005) *MASW- Horizontal Resolution in 2D Shear-Velocity (Vs) Mapping*. KGS Open-File Report 2005-4. Lawrence, KS: KGS.

Parolai S, Bormann P and Milkereit C (2001) Assessment of the natural frequency of the sedimentary cover in the Cologne area (Germany) using noise measurements. *Journal of Earthquake Engineering* 5(4): 541–564. DOI: 10.1142/S1363246901000558.

Pass DG (1994) *Soil characterization of the deep accelerometer site at Treasure Island, San Francisco, California*. MS Thesis, University of New Hampshire, USA.

Passeri F, Foti S, Cox BR, et al. (2019) Influence of epistemic uncertainty in shear wave velocity on seismic ground response analyses. *Earthquake Spectra* 35(2): 929–954. DOI: 10.1193/011018EQS005M.

Piatti C, Foti S, Socco LV, et al. (2013) Building 3D shear-wave velocity models using surface waves testing: The Tarcento basin case history. *Bulletin of the Seismological Society of America* 103(2 A): 1038–1047. DOI: 10.1785/0120120089.

Picozzi M, Parolai S, Bindi D, et al. (2009) Characterization of shallow geology by high-frequency seismic noise tomography. *Geophysical Journal International* 176(1): 164–174. DOI: 10.1111/j.1365-246X.2008.03966.x.

Pilz M, Parolai S, Picozzi M, et al. (2012) Three-dimensional shear wave velocity imaging by ambient seismic noise tomography. *Geophysical Journal International* 189(1): 501–512. DOI: 10.1111/j.1365-246X.2011.05340.x.

Rathje EM, Kottke AR and Trent WL (2010) Influence of input motion and site property variabilities on seismic site response analysis. *Journal of Geotechnical and Geoenvironmental Engineering* 136(4): 607–619. DOI: 10.1061/(ASCE)GT.1943-5606.0000255.

Ritzwoller MH and Levshin AL (1998) Eurasian surface wave tomography: Group velocities. *Journal of Geophysical Research: Solid Earth* 103(B3): 4839–4878. DOI: 10.1029/97jb02622.

Rollins KM, McHood MD, Hryciw RD, et al. (1994) *Ground response on Treasure Island*. US Geological Survey Professional Paper 1551 A: 109–121. Washington, DC. DOI: 10.1016/0148-9062(95)99406-n.

Scherbaum F, Hinzen KG and Ohrnberger M (2003) Determination of shallow shear wave velocity profiles in the cologne, Germany area using ambient vibrations. *Geophysical Journal International* 152(3): 597–612. DOI: 10.1046/j.1365-246X.2003.01856.x.

Strobbia C, Laake A, Vermeer P, et al. (2011) Surface waves: Use them then lose them. Surface-wave analysis, inversion and attenuation in land reflection seismic surveying. *Near Surface Geophysics* 9(6): 503–513. DOI: 10.3997/1873-0604.2011022.

Tao Y and Rathje E (2019) Insights into Modeling Small-Strain Site Response Derived from Downhole Array Data. *Journal of Geotechnical and Geoenvironmental Engineering* 145(7). DOI: 10.1061/(ASCE)GT.1943-5606.0002048.

Teague DP, Cox BR and Rathje EM (2018) Measured vs. predicted site response at the Garner Valley Downhole Array considering shear wave velocity uncertainty from borehole and surface wave methods. *Soil Dynamics and Earthquake Engineering* 113: 339–355. DOI: 10.1016/j.soildyn.2018.05.031.

Thompson EM, Baise LG, Kayen RE, et al. (2009) Impediments to predicting site response: Seismic property estimation and modeling simplifications. *Bulletin of the Seismological Society of America* 99(5): 2927–2949. DOI: 10.1785/0120080224.

Thompson EM, Baise LG, Tanaka Y, et al. (2012) A taxonomy of site response complexity. *Soil Dynamics and Earthquake Engineering* 41: 32–43. DOI: 10.1016/j.soildyn.2012.04.005.

Thornley J, Dutta U, Yang ZJ, et al. (2019) In situ shear-wave velocity measurements at the Delaney Park Downhole Array, Anchorage, Alaska. *Seismological Research Letters* 90(1): 395–400. DOI: 10.1785/0220180178.

Toro GR (1995) *Probabilistic Models of Site Velocity Profiles for Generic and Site-Specific Ground Motion Amplification Studies*. Technical Rep. No. 779574. Upton, NY: Nuclear Energy Brookhaven National Laboratory.

Tran KT and Sperry J (2018) Application of 2D full-waveform tomography on land-streamer data for assessment of roadway subsidence. *Geophysics* 83(3): EN1–EN11. DOI: 10.1190/GEO2016-0550.1.

Tran KT, McVay M, Faraone M, et al. (2013) Sinkhole detection using 2D full seismic waveform tomography. *Geophysics* 78(5): R175–R183. DOI: 10.1190/GEO2013-0063.1.

Virieux J and Operto S (2009) An overview of full-waveform inversion in exploration geophysics. *Geophysics* 74(6): WCC1–WCC26. DOI: 10.1190/1.3238367.

Wen W and Kalkan E (2017) System identification based on deconvolution and cross correlation: An application to a 20-story instrumented building in Anchorage, Alaska. *Bulletin of the Seismological Society of America* 107(2): 718–740. DOI: 10.1785/0120160069.

Yamanaka H, Takemura M, Ishida H, et al. (1994) Characteristics of long-period microtremors and their applicability in exploration of deep sedimentary layers. *Bulletin - Seismological Society of America* 84(6): 1831–1841. DOI: 10.1016/0148-9062(95)99176-x.

Yang Y, Ritzwoller MH, Levshin AL, et al. (2007) Ambient noise Rayleigh wave tomography across Europe. *Geophysical Journal International* 168(1): 259–274. DOI: 10.1111/j.1365-246X.2006.03203.x.

Zalachoris G and Rathje EM (2015) Evaluation of one-dimensional site response techniques using borehole arrays. *Journal of Geotechnical and Geoenvironmental Engineering* 141(12). DOI: 10.1061/(ASCE)GT.1943-5606.0001366.